DOKUZ EYLÜL UNIVERSITY

GRADUATE SCHOOL OF NATURAL AND APPLIED SCIENCES

DESIGN AND CONSTRUCTION OF AN INFRARED TEMPERATURE MEASUREMENT DEVICE THAT WOULD MAKE NONCONTACT MEASUREMENTS FROM THE BODY

by

İsmail Volkan TEKCAN

December, 2014

İZMİR

DESIGN AND CONSTRUCTION OF AN INFRARED TEMPERATURE MEASUREMENT DEVICE THAT WOULD MAKE NONCONTACT MEASUREMENTS FROM THE BODY

A Thesis Submitted to the
Graduate School of Natural and Applied Sciences of Dokuz Eylül University
In Partial Fulfillment of the Requirements for the Degree of Master of
Science of Department of Biomedical Technologies, Biomedical Technologies
Program

by
İsmail Volkan TEKCAN

December, 2014
İZMİR

M.Sc THESIS EXAMINATION RESULT FORM

We have read the thesis entitled "**DESING AND CONSTRUCTION OF AN INFRARED TEMPERATURE MEASUREMENT DEVICE THAT WOULD MAKE NONCONTACT MEASUREMENTS FROM THE BODY**" completed by **İSMAIL VOLKAN TEKCAN** under supervision of **PROF. DR. MEHMET KUNTALP** and we certify that in our opinion it is fully adequate, in scope and in quality, as a thesis for the degree of Master of Science.

Prof. Dr. Mehmet KUNTALP

Supervisor

Doç. Dr. Olcay Akay

(Jury Member)

Metin Sabuncu

(Jury Member)

Prof.Dr. Ayşe OKUR
Director
Graduate School of Natural and Applied Sciences

ACKNOWLEDGMENTS

DESIGN AND CONSTRUCTION OF AN INFRARED TEMPERATURE MEASUREMENT DEVICE THAT WOULD MAKE NONCONTACT MEASUREMENTS FROM THE BODY

ABSTRACT

In this dissertation study, a body temperature measurement device based on an IR (Infra-Red) radiation sensor which detects incoming IR radiation and converts it into a measurable electrical signal is designed and constructed. This device measures body temperature without any contact with the body surface as well as in real time. The IR radiation sensor that is used in this study is Melexis MLX9061 which is produced by "Melexis Microelectronic Systems". In addition, in this study, ATmega328P microcontroller, a product of Atmel Corporation, is used as an embedded system in the Arduino open source code electronic prototype.

The IR radiation measurement sensor is one of the most important parts of the mechanism of the non-contact temperature measurement. These kinds of sensors perceive any changes of temperature that is seen by the focus point or FOV (field of view) of the sensor and produce an electrical signal proportional to the amount of the temperature differences. Also, a temperature measurement system that is based on this kind of sensor is more useful than digital and mercury systems, because these kinds of measurement systems are faster and easier than the digital and mercury types of measurement systems.

Keywords: Infrared electromagnetic radiation, infrared sensors

VÜCUTTAN TEMASSIZ ÖLÇÜM YAPAN KIRMIZI-ALTI SICAKLIK ÖLÇÜM CİHAZININ DİZAYN VE İNŞASI

ÖZ

Bu tez çalışmasında, gelen kırmızı-altı radyasyonu detekte eden ve ölçülebilir bir elektrik sinyaline dönüştüren kırmızı-altı radyasyon sensörü temelli bir vücut sıcaklık ölçüm cihazı tasarlandı ve inşaa edildi. Bu cihaz vücut yüzeyine hiçbir temasta bulunmadan gerçek zamanlı olarak vücut sıcaklığını ölçer. Bu çalışmada kullanılan kırmızı-altı radyasyon sensörü "Melexis Microelektronik Sistemleri" nin ürünü olan Melexis MLX906'dir. Ayrıca bu çalışmada "Atmel Corporation" ın bir ürünü olan ATmega328P mikro kontrolör, açık kaynak kodlu elektronik prototip olan arduinoya gömülü şekilde kullanılmıştır.

Kırmızı-altı radyasyon ölçüm sensörleri temassız sıcaklık ölçüm mekanizmasının en önemli kısımlarından biridir. Bu tip sensörler, sensörün FOV (field of view)' u veya odak noktası tarafından görülen herhangi sıcaklık değişimini algılayıp, bu sıcaklık farkının miktarıyla orantılı elektrik sinyali üretirler. Ayrıca, bu çeşit sensör temelli bir sıcaklık ölçüm sistemi dijital ve civalı sistemlerden daha kullanışlıdır, çünkü bu çeşit ölçüm sistemleri dijital ve civalı tip ölçüm sistemlerden daha hızlı ve daha kolaydır.

Anahtar kelimeler: Kırmızıaltı elektromanyetik radyasyon, kırmızıaltı algılayıcılar

CONTENTS

LIST OF FIGURES

CHAPTER ONE
INTRODUCTION

Human eyes can see only visible light that exists on the visible region on the electromagnetic spectrum or radiation spectrum. Although visible range can be seen by human eyes, on the spectrum, visible region has a small area, and the invisible region which includes invisible lights has the rest of the spectrum. Also, all electromagnetic waves carry information from objects or environment. For example, in the visible region, reflected light from an object carries its vision information, and similarly IR radiation emitted from an object carries its temperature information. In addition, X-rays transmitted from a human body carry vision information from the inside of the human body in radiological imaging, and γ-rays are used for similar reason in nuclear medicine imaging.

In this chapter, electromagnetic waves, electromagnetic radiation spectrum, IR radiation and black body radiation were expressed. Also, the physical basics and principles of the black body radiation were shown simply as theoretic information.

1.1 The Electromagnetic Radiation Spectrum

In general, light is defined as a form of energy that displays characters of both of waves and particles. This is called duality of the light in quantum physics. Also, light is characterized as electromagnetic radiation that has electric and magnetic field which are perpendicular to each other. Figure 1.1 (Harvey, 2008) shows electromagnetic radiation components that are plane-polarized in x-y coordinate system.
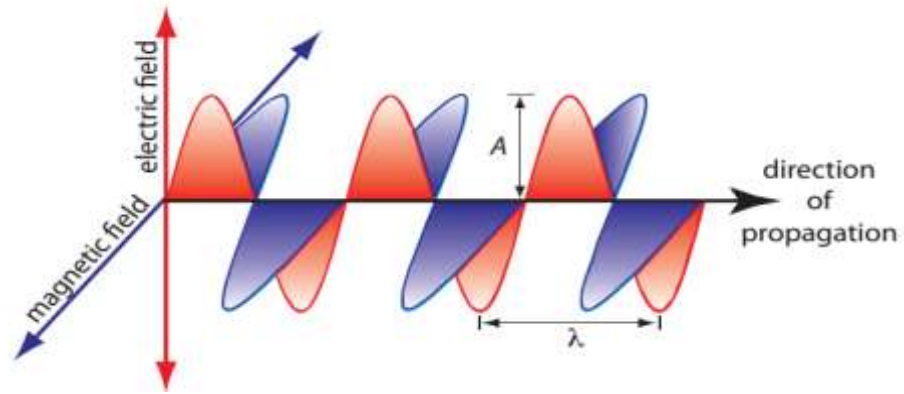
Figure 1.1 Polarized electromagnetic radiation; radiation amplitude, A and its wavelength, λ (Harvey, 2008)

Also, the amplitude of the electromagnetic waves is given by the equation shown below;

$$A = A_0 \sin(2\pi v + \varphi) \qquad (1.1)$$

In this equation, A_0, v and φ symbolize maximum amplitude, frequency and phase angle of the electromagnetic wave. And, frequency of the wave is defined with Equation 1.2 that is shown below.

$$v = \frac{c}{\lambda}, c: speed\ of\ light, \lambda: \text{wavelength of the electromagnetic wave} \qquad (1.2)$$

Moreover, the energy of the radiation that has wavelength as λ is shown with Equation 1.3.

$$E = \frac{hc}{\lambda}, E: energy\ of\ the\ electromagnetic\ wave \qquad (1.3)$$

$h = 6.626 \text{ x } 10^{-34} \text{ Js}$

All electromagnetic radiation in the electromagnetic spectrum which is shown in Figure 1.2 (Jones, 2010) abides by the principles of diffraction, refraction, reflection and polarization. Also, all electromagnetic radiation expansion speed equals to the speed of light in space (Harvey, 2008).

2
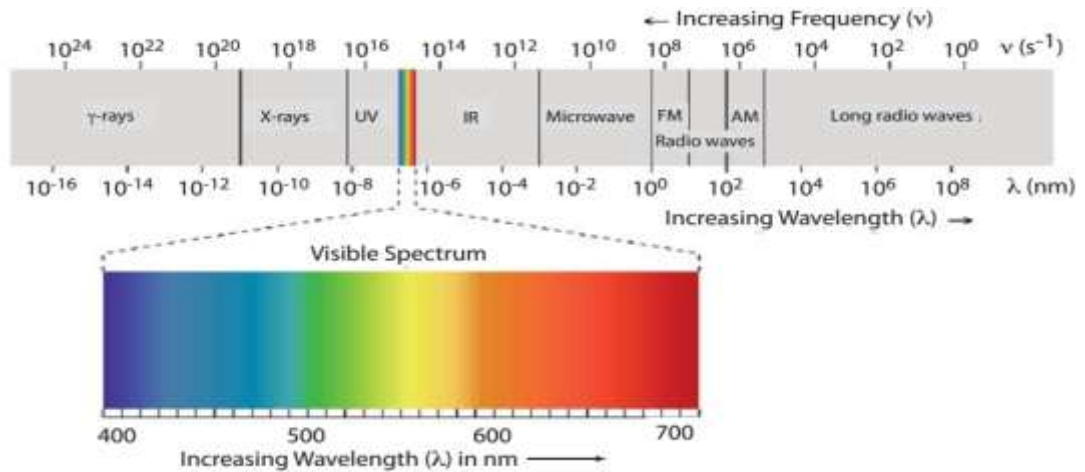
Figure 1.2 Electromagnetic spectrum (Harvey, 2008)

1.2 The Infra-Red Radiation Spectrum

One of the invisible lights on the spectrum is IR (infra-red) radiation that is emitted from objects whose temperatures are above the absolute zero. IR radiation was defined in 1800s first by Sir William Hershel.

If an object has a temperature above absolute zero (−273.16°C (or 0 K)), all atoms and molecules makes vibration kinetically. These vibrations create electromagnetic waves that are released from the object at the speed of light. The energy of the electromagnetic waves is in the thermal range between wavelength of 0.1 µm and 1000 µm, as shown in Figure 1.3 (Jones, 2010). This range is called thermal range, because this wavelength range includes thermal information of an object that emits IR radiation due to its molecular vibration kinetically. When the object temperature is above absolute zero, its vibration produces temperature, and this temperature spreads as thermal radiation. Owing to the fact that this thermal radiation is a kind of electromagnetic radiation; it has 'E' energy, 'υ' frequency and 'λ' wavelength. It is concluded from the expression, thermal range is determined by the thermal radiation wavelength range. That's why; this range is called the thermal range.
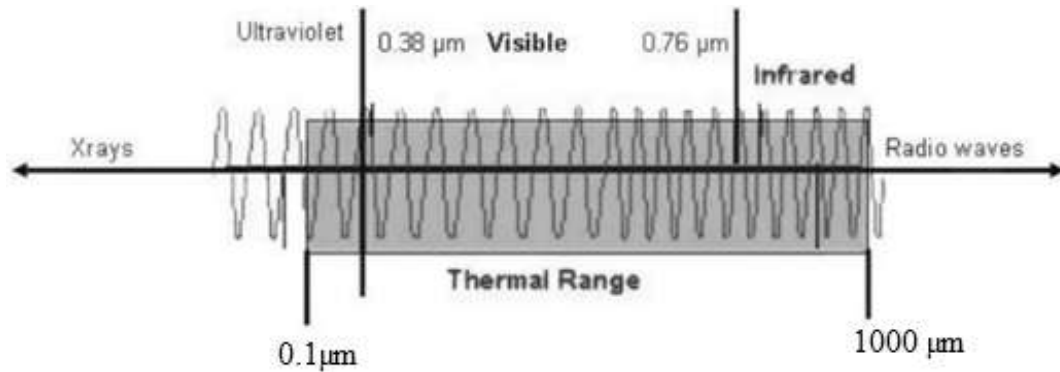
Figure 1.3 Thermal range of electromagnetic spectrum (Jones, 2010)

The infrared radiation locates in a limited part of the electromagnetic spectrum: Its boundaries starts at about 0.70 μm and ends at wavelengths of nearly 1000 μm. The range of wavelength between 0.70 and 14 μm are important for infrared temperature measurement. Since outside of this wavelength range, the energy level that is expected to sense by detectors is very low according to the detection ability of the detectors to detect the radiation sufficiently. In other words, out of this wavelength range, wavelength increases and it causes the decreasing of the emitted radiation energy. In about 1900, physical basics of the electromagnetic spectrum were exactly defined by Wien and Kirchhoff, Stefan, Boltzmann, Planck (Jones, 2010).

In addition, the IR range (IR spectrum) of the electromagnetic spectrum can be divided into three more segments inside of itself in terms of wavelength, and their boundaries are nearly 0.8 μm to 2.0 μm (near IR), 2.0 μm to 5.6 μm (middle IR), 7.5 μm to 15 μm (far or long-wave IR) (Jones, 2010). In this study these segments are not interested, so details of them are not expressed.

1.3 The Black Body Radiation

An ideal black body is an object that completely absorbs all incoming radiation without showing neither transmissivity nor reflection, and it radiates in all directions at all wavelengths. Also, the emitted radiation concentration is independent of the angles that waves spread. The black body is momentous to find out the basis of the physical fundamentals of non-contact temperature measurement and to calibrate the infrared thermometers.

The most successful and classical approach to the structure of the black body is to associate it with a cavity that takes all radiation from the environment to a hollow via a small hole. Because of any incoming radiation would get inside the cavity via the small hole and then a lot of time it reflects on the internal surface, and at last be exactly absorbed by the surface layer of the cavity inside, this cavity would be considered to behave as a near perfect absorber. The result of that the cavity inside walls are continuously radiating and reabsorbing their own radiation, thermal equilibrium occurs quickly between all radiations inside the cavity with the cavity, and moreover the radiation that gets out from the cavity through the small hole should have the same spectral dependence as all other perfect absorbers at the same temperature.
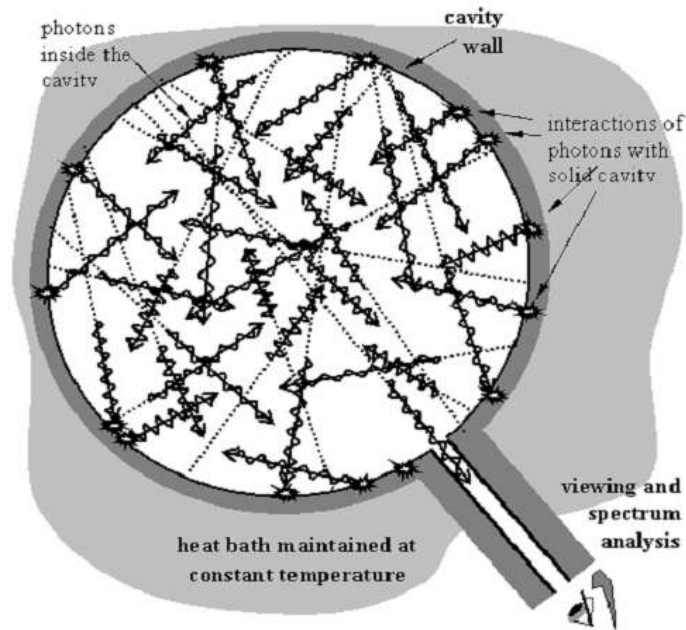
Figure 1.4 Classical representation of black body (Johnson, 2012)

"Equipartition theorem" expresses that every molecule of an object at thermal equilibrium should save average energy equal to Equation 1.4 for every available "degree of freedom (or "mode"). In this equation, T is the absolute temperature, and it is the reason of kinetic energy that the every particle of the object has (Mallinckrodt, & Pomona, 2010); (Equipartition theorem, n.d.).

$$E_{avg} = \frac{1}{2}k_B T \qquad (1.4)$$

In this equation, T is the system's absolute temperature and k_B is the Boltzmann constant that is given by $k_B=1.38\times10^{-23}$J/K.

Equation 1.4 can be generalized for any systems whose degree of freedom equals "n" that goes on discretely from 1 to infinity, and the systems that are composed of "N" particles (Mallinckrodt, & Pomona, 2010).

$$E_{avg} = \left(n - \frac{1}{2}\right) Nk_BT \qquad (1.5)$$

Using a thermal cavity that has a little hole at one end, generation of the black body is so simple. If the cavity is heated until it reaches an absolute temperature, inner walls of the cavity have equilibrium and the cavity spreads temperature to out of it. And, at this temperature the hole radiates such as an ideal black body. Depending on materials and the geometric structures, constructed black body can be used for each temperature range and application according to appropriate purposes. If the measuring device is pointed on the hole, it can give the information of temperature emitting from inside of the cavity as black radiation which can be used for calibrating the temperature measurement system.
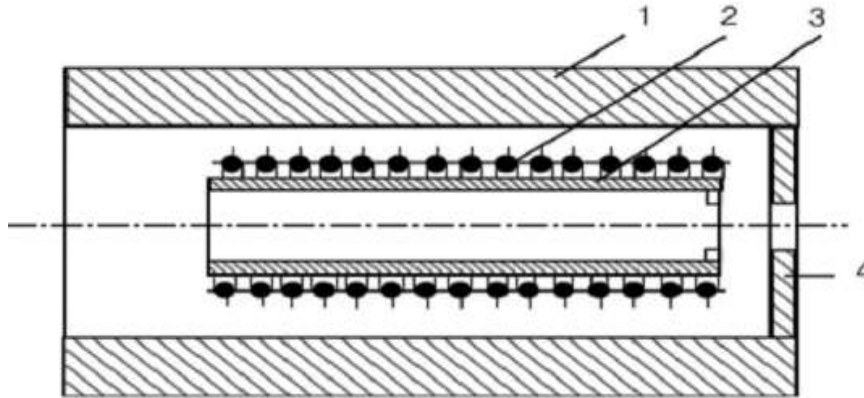
Figure 1.5 Drawing of a black body: 1 - ceramic conduit, 2 - heating, 3 - conduit made from Al_2O_3, 4 – aperture (Optris, n.d.)

1.4 Radiation Principles of a Black Body

In this section, quantum mechanical approach is required, because of the understanding and determination of the black body radiation spreads. The Equation

1.6, which is shown below, is the classical simple harmonic oscillator equation, and its general solution is given by Equation 1.7.

$$\frac{d^2\psi}{x^2} = -k^2\psi, \ \ k = \frac{\sqrt{2mE}}{h} \tag{1.6}$$

$$\psi(x) = A\sin kx + B\cos kx \tag{1.7}$$

A and B are arbitrary constants of the equation and they are calculated from boundary conditions that are given in the problem. In this case, it is assumed that the boundary conditions of the problem are $\psi(0)=0$, and $\psi(a)=0$.

$$\psi(0) = A\sin 0 + B\cos 0 \ \rightarrow B = 0$$

$$\psi(x) = A\sin kx \tag{1.8}$$

$$\psi(a) = A\sin ka \ \rightarrow \text{A} = 0 \text{ (trivial, non-normalizable solution), or } \sin ka = 0$$

It means, $ka = 0, \pm\pi, \pm2\pi, \pm3\pi, ...$

 However, k = 0 takes the Equation 1.8 to $\psi(x) = 0$, so it is unacceptable. Also, since $\sin(-\theta) = -\sin(\theta)$, negative solutions are absorbed in A. Thus, all acceptable distinct solutions are shown below.

$$k_n = \frac{n\pi}{a}, \quad \text{n} = 1,2,3,... \tag{1.9}$$

Until here, the classical simple harmonic oscillator equation was solved and k_n is determined as 'n' dependent. In here, k symbolizes the number of waves, and n is the degrees of freedom or resonant modes.

The Equation 1.9 shows that degrees of freedom for waves on a string of length L have wave numbers that can be given by $k_n = \frac{2\pi}{\lambda} = \frac{n\pi}{L}$. In a rectangular box with volume V = L_x x L_y x L_z, the degrees of freedom for three-dimensional waves (acoustic, electromagnetic, etc.) have wave vectors shown below (Griffiths, 2004).

$\vec{k} = k_x \check{x} + k_y \check{y} + k_z \check{z}$, with $k_x = \frac{n_x \pi}{L_x}$, $k_y = \frac{n_y \pi}{L_y}$, and $k_z = \frac{n_z \pi}{L_z}$.

Figure 1.6 (Mallinckrodt & Pomona, 2010) shows graphical representation of these modes in three-dimensional k-space on a lattice. Furthermore, the unit "volume" in k-space that is determined by closest neighbors on the lattice is given by Equation 1.10, and V is the physical volume of the rectangular cavity in this equation.
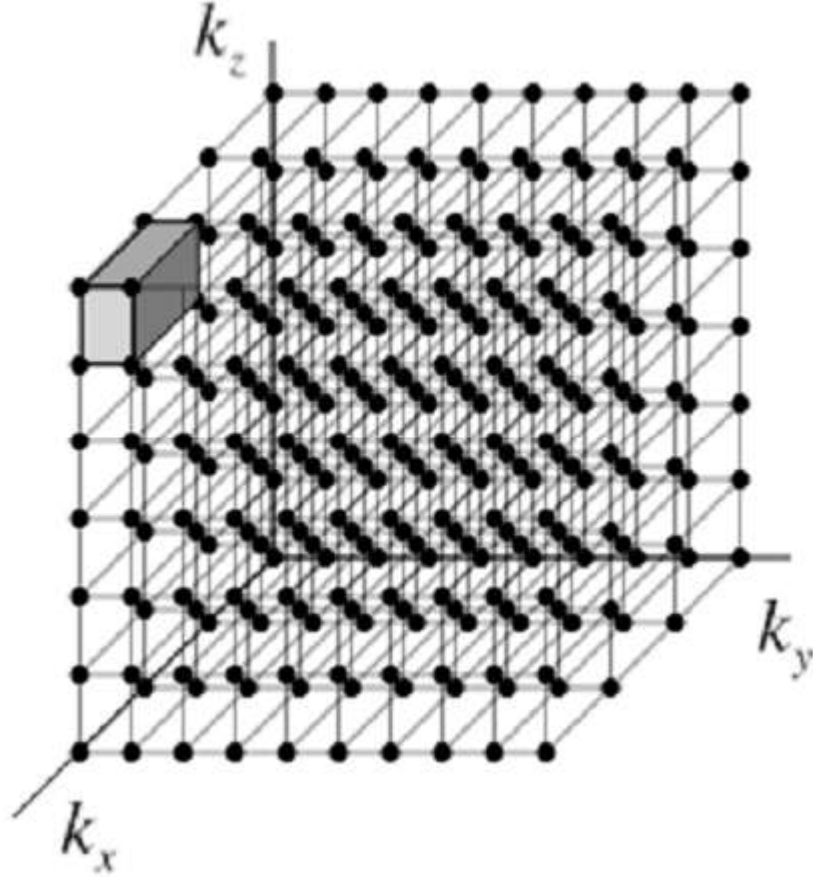
Figure 1.6 Representation of the modes in three-dimensional k-space (Mallinckrodt & Pomona, 2010)

$$\Delta V = \frac{\pi^3}{L_x L_y L_z} = \frac{\pi^3}{V} \tag{1.10}$$

The number of modes (degrees of freedom), $N_k(k)dk$, and wave vectors having magnitudes between k and k+dk are needed to be known, so that the spectral density of the radiation field can be found. Figure 1.7 (Mallinckrodt & Pomona, 2010) shows

one octant of a spherical shell in k-space. ΔV_k is fit in the shell, and Equation 1.11 can be written, because each ΔV_k is correlated with one resonant value of $\vec{k}$ and each resonant value of $\vec{k}$ is correlated with two resonant modes. Here, ΔV_k is the number of unit volume.
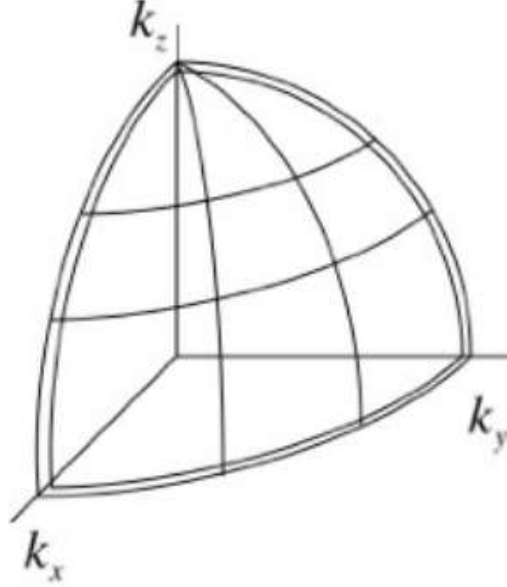
Figure 1.7 One octant of a spherical shell in three-dimensional k-space (Mallinckrodt & Pomona, 2010)

$$N_k(k)dk = 2 \times \frac{(volume\ of\ shell\ in\ k-space)}{\Delta V_k} = 2 \times \frac{(4\pi k^2 dk)/8}{\pi^3/V} = \frac{V}{\pi^2}k^2 dk \qquad (1.11)$$

Equation 1.12 gives, $u_k(k)dk$, the energy per unit volume saved in degrees of freedom and wave vectors that have magnitudes between k and k+dk. It means, each degree of freedom of the electromagnetic field (radiation field) should be expected to save, on average, kT of energy ($\frac{1}{2}$kT in electrical energy and another $\frac{1}{2}$kT in magnetic energy). Furthermore, the result neither depends on the cavity dimensions, nor on the shape of the cavity. Also, the spectral energy density in terms of wavelength can be obtained as shown in Equation 1.13. This is a classical calculation of the spectral energy density in the cavity radiation field (Mallinckrodt & Pomona, 2010).

$$u_k(k)dk = \frac{N_k(k)dk}{V}(k_B T) = \frac{k_B T k^2}{\pi^2}dk \qquad (1.12)$$

9

k_B: Boltzmann constant that is given by k_B=1.38×10^{-23}J/K

k: Number of wave

dN: Number of states between k and $k + dk$

N: Number of vibration

V: The physical volume of the rectangular cavity

$N_k(k)dk$: Wave vector

$$u_\lambda(\lambda) = u_k \left(\frac{2\pi}{\lambda}\right) \left|\frac{dk}{d\lambda}\right| = \frac{8\pi k_B T}{\lambda^4}$$ (1.13)

All electromagnetic waves travel at the speed of light in space, and they can be considered energy packets carrying their energy. Equation 1.14 gives a classical calculation of black body spectral radiance coming out from the hole, and it is known as "The Rayleigh-Jeans Radiation Law". At long wavelengths, the Rayleigh-Jeans law represents the experimental data fairly well, but it cannot be possible at smaller wavelengths regardless of the temperature. And, the failure of the Rayleigh-Jeans law at short wavelengths (high frequencies) is called the "ultraviolet catastrophe."

$$I_\lambda(\lambda) = \frac{u_\lambda}{4} c = \frac{2\pi c k_B T}{\lambda^4}$$ (1.14)
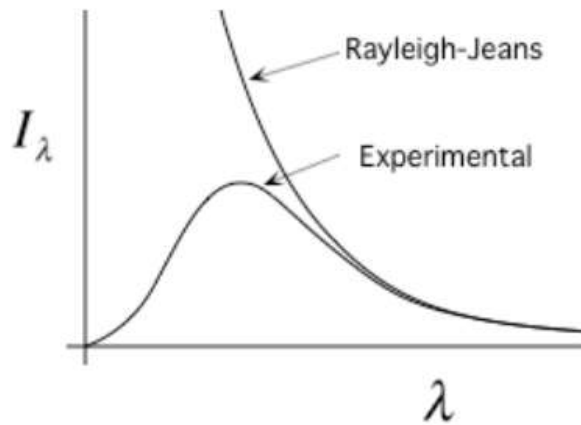
Figure 1.8 Behavior of the Rayleigh-Jeans law (Mallinckrodt & Pomona, 2010)

As a result of the "ultraviolet catastrophe", the equipartition theorem is disrupted for high frequency radiation. However, Max Planck explains that the degrees of freedom can only save integer multiples of a fundamental energy quantum which is

proportional to the frequency of the degree of freedom. It means the energy of a degree of freedom can only assume values given by Equation 1.15. The average energy calculation in a degree of freedom is obtained using another result from classical thermodynamics that means the likelihood of a system at thermal equilibrium saving an energy E is proportional to the "Boltzmann factor" that is given by $e^{-E/k_B T}$. Also, the average energy that is saved in a degree of freedom is shown in Equation 1.16 (Mallinckrodt & Pomona, 2010).

$$E = n(h\nu), \ n = 0,1,2,\dots \tag{1.15}$$

$$\langle E \rangle = \frac{e^{-\frac{0}{k_B T}}(0) + e^{-\frac{h\nu}{k_B T}}(h\nu) + e^{-\frac{2h\nu}{k_B T}}(2h\nu) + \cdots}{e^{-\frac{0}{k_B T}} + e^{-\frac{h\nu}{k_B T}} + e^{-\frac{2h\nu}{k_B T}} + \cdots} = \frac{\sum_{n=0}^{\infty} n\varepsilon e^{-n\varepsilon}}{\sum_{n=0}^{\infty} e^{-ne}} \tag{1.16}$$

➔ $\varepsilon \equiv h\nu/k_B T$,

➔ $-\varepsilon \frac{d}{d\varepsilon} \ln \sum_0^{\infty} e^{-n\varepsilon} = \frac{-\varepsilon \frac{d}{d\varepsilon} \sum_0^{\infty} e^{-n\varepsilon}}{\sum_0^{\infty} e^{-n\varepsilon}} = \frac{-\sum_0^{\infty} \varepsilon \frac{d}{d\varepsilon} e^{-n\varepsilon}}{\sum_0^{\infty} e^{-n\varepsilon}} = \frac{\sum_0^{\infty} n\varepsilon e^{-n\varepsilon}}{\sum_0^{\infty} e^{-n\varepsilon}}$,

➔ $\sum_0^{\infty} e^{-n\varepsilon} = 1 + e^{-\varepsilon} + (e^{-\varepsilon})^2 + \dots = (1 - e^{-\varepsilon})^{-1}$,

Finally; $\langle E \rangle = k_B T \left[-\varepsilon \frac{d}{d\varepsilon} \ln(1 - e^{-\varepsilon})^{-1} \right] = \frac{k_B T \varepsilon e^{-\varepsilon}}{(1 - e^{-\varepsilon})} = \frac{h\nu}{e^{h\nu/k_B T} - 1}$ \hfill (1.17)

As a result, using Equation 1.14 and 1.17, Equation 1.18 is obtained. It describes the spectral specific radiation, $I_\lambda(\lambda)$, of the black body into the half space depending on its temperature T and the wavelength λ.

$$I_\lambda(\lambda) = \frac{2\pi c}{\lambda^4} \left(\frac{hc/\lambda}{e^{hc/\lambda k_B T} - 1} \right) = \frac{2\pi h c^2}{\lambda^5 (e^{hc/\lambda k_B T} - 1)}, \ h = 6.63 \times 10^{-34} J.s \tag{1.18}$$

Thus, Equation 1.18 can be written as shown below;

$$I_\lambda(\lambda) = \frac{C_1}{\lambda^5} \frac{1}{e^{C_2/\lambda T} - 1} \tag{1.19}$$

$C_1 = 3.74 \times 10^{-16} W.m^2$

$C_2 = 1.44 \times 10^{-2} K.m$

λ: Wavelength of the radiation

I_λ: Spectral specific radiation (or flux of radiation) of a black body

T: Absolute temperature
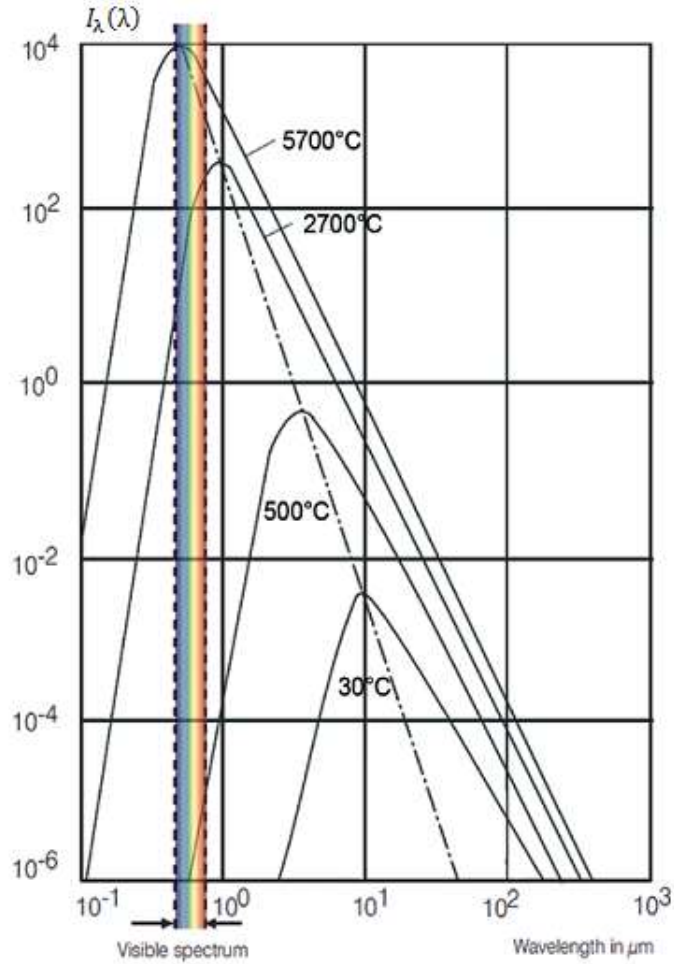
Figure 1.9 Spectral specific radiation I_λ of the black body depending on the wavelength; 30°C = 303.16 °K, 500°C = 773.16 °K, 2700°C = 2973.16 °K, 5700°C = 5973.16 °K (Optris. n.d.)

When the temperature is increased, the maximum of the spectral specific radiation goes to shorter wavelengths. Besides, some correlations can be derived as Equation 1.18 or 1.19. As known Stefan-Boltzmann-Law, the emitted radiation value of the body as a whole can be obtained by integrating the spectral radiation density for all wavelengths from 0 to infinity.

$$I = \int_0^\infty I_\lambda(\lambda)d\lambda = (\frac{2\pi^5 k_B{}^4}{15c^2 h^3})T^4 = (5.6704 \dots \times 10^{-8} \frac{W}{m^2.K^4})T^4 \tag{1.20}$$

12

$$\rightarrow \quad \frac{dI_\lambda}{d\lambda} = 0 , \quad \frac{ye^y}{e^y-1} = 5 , \quad y = \frac{hc}{\lambda k_B T} = 4.96511 \ldots$$

$I_\lambda = \sigma . T^4$; (Stefan-Boltzmann-Law) $\hfill$ (1.21)

$\sigma = 5.67 \times 10^{-8} \, \mathrm{Wm^{-2}K^{-4}}$

I_λ: Spectral specific radiation (or flux of radiation) of a black body

σ: Stefan-Boltzmann constant

T: Absolute temperature

Equation 1.21 says that spectral specific radiation (or flux of radiation) of a black body is proportional to power of its absolute temperature.

Moreover, Equation 1.22 shows Wien's displacement law that is derived from Planck's formula by differentiation. This law says that the wavelength, which belongs to maximum radiation, changes towards the range of short wavelengths when the temperature increases.

$$\lambda_{max} T = \frac{hc}{(4.96511)k_B} = 2.8978 \, mmK \hfill (1.22)$$

λ_{max}: The peak wavelength of the thermal radiation that has absolute temperature of T (as shown in Figure 1.1)(mm)

T: The absolute temperature of the object (°K)

h: Planck constant

c: Speed of light

$c = 2.99792 \times 108$ m/s

$h = 6.626 \times 10\text{-}34$ Js

Using this equation, it is possible to calculate the temperature of a radiation source from a knowledge of its wavelength of emitted radiation.

IR region's boundaries start at the visible range of about 0.70 µm and ends at wavelengths of nearly 1000 µm. However, the range of wavelengths between 0.70 and 14 µm usually are important for infrared temperature measurement. Using this

information and Equation 1.22, the temperature range which can be detected by IR radiation sensors is calculated as shown below. All of those theoretical parts are important to calculate a temperature measurement range of IR radiation sensors. Also, Table 1.1 shows some IR radiation wavelength with their corresponded temperatures.

Wavelength range is 0.7 and 14 µm; λ_1= 0.7 µm, λ_2= 14 µm

From Equation 1.22; T_1=4139.85° K = 3866.69° C and T_2= 206.98° K = -66.18° C

Table 1.1 Some IR radiation wavelengths with their corresponding temperatures

Wavelength (µm)	Temperature (°K)
10	2897.8
20	1448.9
100	289.78
200	144.89
1000	28.978

In this chapter, as a result of all of these calculations it is seen that the amount of spectral specific radiation of an object which has an absolute temperature above zero is found using Equation 1.21. In addition, the measurement ranges of detectors which were expressed in Chapter 2 and designed Chapter 3 are determined using Equation 1.22.

CHAPTER TWO
INFRARED THERMAL DETECTORS

In this chapter, some general information is given about detectors which are used currently for IR temperature measurement. Besides, especially, the basic principle of the thermopile detector which is one of the thermal detector types was expressed, due to its used in the designed IR radiation thermometer.

2.1 General Structure and Operation of Infrared Thermometers

At the first sight of the human eye, it can be considered a kind of radiation sensor. Electromagnetic radiation spectrum was shown in Chapter 1, and it is easy to see that even the visible range of the spectrum is a radiation field whose wavelengths are between 400 and 700 nm. For an object to be seen by human eyes, the radiation that is in the visible range of the spectrum must reflect from the object and must reach to the eyes. The eye has a lens to focus the radiation flux emitted from the source onto the retina. The incident radiation that comes from the lens stimulates the retina and produces a signal that is traveled to the brain. After that, this signal is processed by the brain, in order to generate a view of the object that photons come from. This is similar to the mechanism of the IR sensor system.

The general structure of an IR thermometer is shown in Figure 2.1 (Optris, n.d.). The incoming radiation is focused onto the IR sensor by optic lens of the system. The sensor produces an electrical signal which then is amplified, converted and processed to take information from the signal. After the signal processing, processor transforms the signal into an output value proportional to the object temperature, and it is demonstrated in the display.
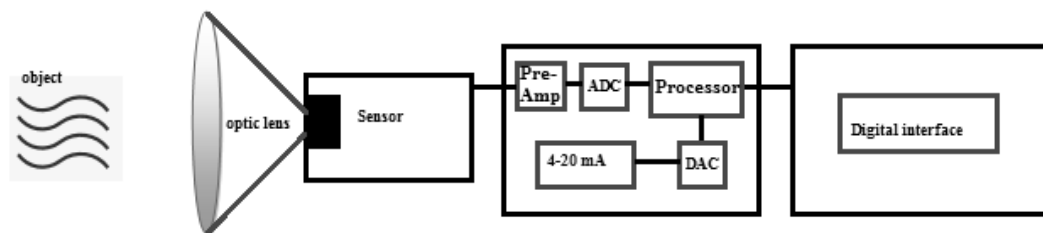
Figure 2.1 General structure of the IR thermometer

Consequently, measurement of an object temperature can be accomplished mainly in three steps.

1) Receiving IR radiation from an object to the lens

2) Generation of an electrical signal from the received IR radiation

3) Signal processing, linearization and output of temperature information.

2.2 Infrared Detectors

IR radiation detectors are generally in two different forms which are called photon (or quantum) and thermal detectors. However, all of them have the same purpose of converting incoming photon flux into an electrical signal, in order to generate temperature information. Figure 2.2 shows the general classification of the IR detectors.
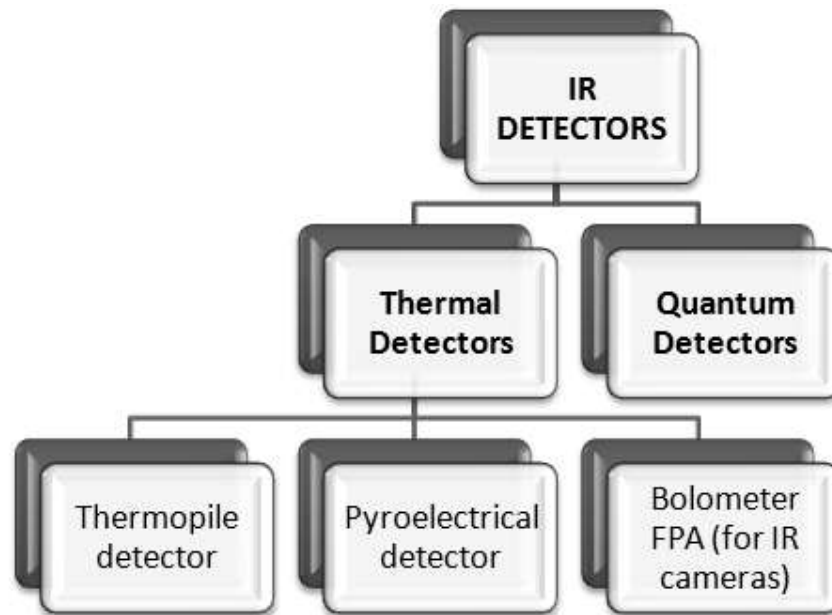
Figure 2.2 Classification of IR detectors

2.2.1 Quantum Detectors

The process of the quantum detectors which generally consist of a semiconductor crystal is based on converting photon energy into released energy of electrons (from valence band to conduction band). The amount of energy that is needed to transport an electron from the valence band to the conduction band is determined by the bandwidth of the crystal lattice. If the energy, which is due to the incoming IR radiation, is sufficient to rip off the electron from valence band and transport it from the valence band to the conduction band, the electron moves back to valence band after arriving at conduction band. This movement of the electron causes changing in electrical properties of the crystal. These electrical property variations of the crystal are the reason of producing an electrical voltage which is measured to determine the amount of IR radiation that is directly related with the object temperature.

The quantum detector counts photons that can reach into detector and have enough energy to free a bound electron. Also, owing to the fact that the quantum detector is evenly sensitive to all photons that are able to free a bound electron, all of these types of detectors show a quite uniform response to all incoming photons up to a certain wavelength, and out of this specific wavelength the photon does not have enough energy to free enough electrons for producing a signal that carries temperature information.

In Chapter 1, it is shown that IR radiation occurs from a flux of the quantum-mechanical elements of all electromagnetic radiation which is called photons. Also, Equation 1.3 gives the energy (E_p) of a photon (Bronzino, 2006).

There are two types of quantum detectors that are produced;

•Photoconductive

•Photovoltaic

2.2.1.1 Photoconductive Detectors

In the crystal material, the photons which are sourced by IR radiation lead to excite valence electrons and let them free from the valence band. After exciting and getting free, these electrons move freely in the crystal. When the crystal is used in the bias circuit having an electric field, E, increasing of the amount of these electrons which are generated by the photon flux causes an increase in the current. This process is based on the photoconductive detector mechanism.
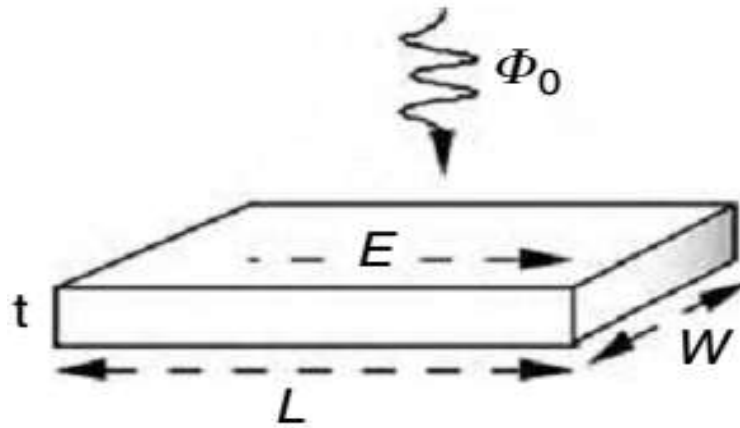
Figure 2.3 Photoconductive detector geometry, $\emptyset_0$: Photon flux L: Detector element's dimension length W: Detector element's width t: Detector element's thickness (Bronzino, 2006).

2.2.1.2 Photovoltaic Detectors

In this type of detector, photo-excited carriers are aggregated by a diode junction. This situation effectuates the basic mechanism of photovoltaic detectors which are the most commonly used photon detectors for imaging arrays. Figure 2.5 (Bronzino, 2006) shows this type of detector structure.

All quantum detectors consist of a p-n junction. Photons that come from the object are absorbed in the n-type layer of the detector material. Those absorbed photons generate a pair of charge carriers called an electron and a hole. In this part of the

detection mechanism the hole passes to the p-type side of the junction producing a photocurrent.

2.2.2 *Thermal Detectors*

A thermal detector absorbs incoming radiation flux and this absorption causes an increase in detector's temperature which changes a measurable physical feature of the sensitive material. The change of the feature produces electrical signal similar to quantum detector. This signal is analyzed and used for reaching temperature information of the object.

This type of detector generally has a special surface that is completely black in order to be sensitive to all wavelengths. The reaction of the detector depends on the increasing inner temperature of itself, naturally it responds slowly compared to the quantum detectors.

2.2.2.1 Thermopile Detectors

A thermopile which consists of a few serially connected thermocouples junction pairs can be used as a measurement sensor for temperature. Each thermocouple junction pair has two junctions that are named the active junction (or hot junction) and the reference junction (or cold junction). The active junction of the thermocouple absorbs the thermal radiation, and increases its temperature depending on the incoming IR radiation. The temperature difference between the active junction and the reference junction produces an electromotive force directly proportional to the temperature differences. The thermoelectric effect which can be expressed as a phenomenon involving an inter-conversion of heat and electrical energy is based on thermocouple mechanism. A voltage that is proportional to the temperature difference between the active and reference junctions is generated. Actually, the active and reference junctions are affiliated by alternating n-type and p-type materials, called "Arms" which is the Seebeck effect occurring between the junctions.

In the second decade of the 19th century, Thomas Johann Seebeck (1770-1831), discovered that when the temperature difference of the junctions of a closed circuit that consists of two different conductors A and B can be kept, a small electric current flows in this circuit depending on the magnitude of the temperature difference. A thermocouple is created by these two different conductor materials connected in series. Seebeck's experimental results showed that the temperature difference ΔT between the junctions is proportional to the output voltage. Figure 2.7, (Wang & Li, 2011), shows general representation of an elementary thermocouple structure. In this figure, T_1 and T_2 represent temperature of the "hot" point and the stable reference temperature of the "cold" point, respectively.
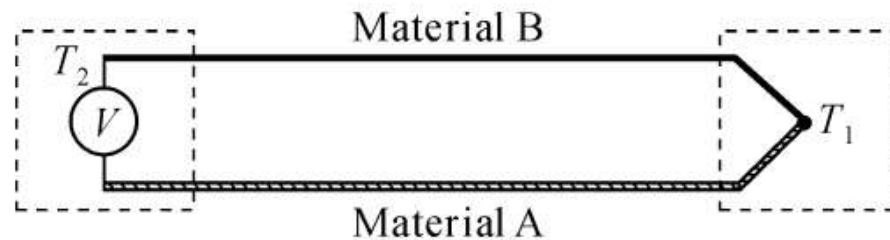
Figure 2.4 Schematic showing an elementary thermocouple (Wang & Li, 2011)

In a thermocouple, the charge carriers of the materials pass to opposite sides when a temperature difference occurs. Hot carriers which exist on the hot junction side diffuse from the hot side to the cold side, because there is a lower intensity of hot carriers at the cold side of the material. The cold carriers which exist on the cold junction sides diffuse from the cold side to the hot side due to the same reason (Weckmann, 1997; Wang & Li, 2011).

The important point is the electromotive force (emf (V)) that is seen in an open circuit is obtained from the measuring junction (active junction) by the thermocouple to cut the flow of electric current. If the circuit is opened, E_{AB} (emf), is called the relative Seebeck emf (RSE) (or Seebeck voltage). For an ideal thermocouple, the emf, E_{AB} (V), is proportional to the temperature difference that is given by ΔT (K) between the two junctions. Equation 2.4 shown below gives the relation between

Seebeck voltage, E_AB, and temperature difference, ΔT. Also, Seebeck effect is illustrated in Figure 2.8 (Weckmann, 1997).

$$E_{AB} = S_{AB}\Delta T ,$$ (2.4)

S_{AB}: *Seebeck coefficient.*
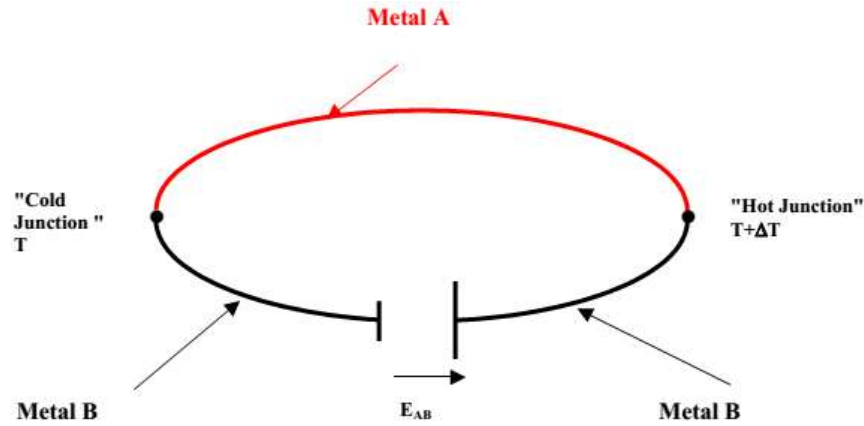
Figure 2.5 Seebeck effect (Weckmann, 1997)

Furthermore, the description of the Seebeck coefficient is the potential difference per unit temperature difference, and it can be given by Equation 2.5. Also, this coefficient depends on the temperature, and the materials that form the thermocouple. Thus, the Seebeck coefficient is calculated using the absolute difference in the coefficients of the two conductors that create the thermocouple, as shown in Equation 2.6.

$$S_{AB} = \frac{\Delta V}{\Delta T}, \quad (\frac{\mu V}{K})$$ (2.5)

$$S_{AB} = |S_A - S_B|$$ (2.6)

S_{AB}: Absolute difference between Seebeck coefficient of the A and B matters

ΔV: Potential difference between A and B matters

ΔT: Temperature difference between A and B matters

S_A: Seebeck coefficient of the A

S_B: Seebeck coefficient of the B

To sum up, the amount of generated voltage can be interpolated as a measure of temperature difference. The relationship between the emf and the temperature difference is given by the Seebeck coefficient as shown before. Also, temperature-emf characteristics of the thermocouples are nearly linear.

In a circuit, when a current flows across a junction of two different conductive materials, heat is released or absorbed depending on the direction of the current on the contrary the Seebeck current. This effect is called Peltier effect. It was discovered by Jean Charles Athanase Peltier in 1834. The thermoelectric refrigeration or heating is based on this effect that is illustrated in Figure 2.9 (Weckmann, 1997).

$$P = P_{AB}I \quad [W] \tag{2.7}$$

P: The rate of heat released or absorbed
I: electric current flowing in the conductor
P_{AB} (V): The relative Peltier coefficient
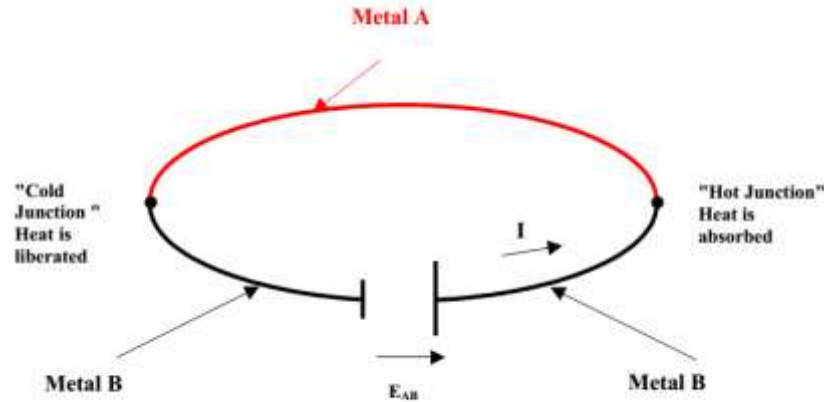
Figure 2.6 Peltier effect (Weckmann, 1997)

At last, when a temperature gradient occurs in the conductor, and if current flows through a single conductor, depending on the relative direction of the gradient and the current, an energy interaction occurs and power is either absorbed or released. Thus, heat is absorbed when an electric current flows in the opposite direction as the heat flows; otherwise it is released. This is called Thomson effect that is discovered in 1852 by Thomson. Equation 2.8 shows the power P' absorbed or rejected per unit

length (W/m) is proportional to the product of the electric current I (A) and the temperature gradient dT/dx (K/m).
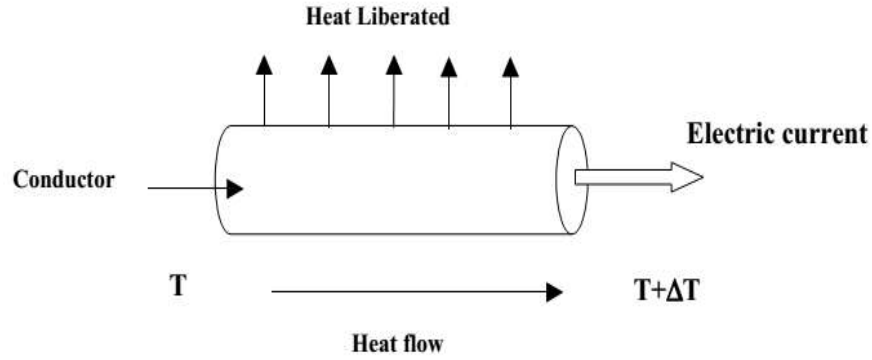
Figure 2.7 Thomson effect (Weckmann, 1997)

$$P' = \sigma(T)I\frac{dT}{dx} \hspace{5cm} (2.8)$$

P': power that is absorbed or released per unit length (W/m)

σ: The Thomson coefficient that depends on the temperature, T

As a result of all these mechanisms, owing to a temperature difference occurring between the two junctions of the thermocouple junction pair, when the thermocouples are connected in series; they can be used as a sensor of IR radiation.

In a thermocouple, when the process that causes voltage production is fulfilled, the amount of generated voltage usually is on the order of a tenth of a microvolt per degree Celsius of temperature difference for a single junction pair. Surely, this is not sufficient for getting an electrical signal. In order to increase this output voltage, a lot of junction pairs are connected in series. Such a device is named a thermopile. If 'n' thermocouple junction pairs are added in series for increasing output voltage, the gain is given by Equation 2.9. Figure 2.11 (Weckmann, 1997) shows an illustration of a thermopile (Weckmann, 1997).

$$\Delta V = nS(T)\Delta T \hspace{5cm} (2.9)$$

ΔV: Potential difference between A and B matters

ΔT: Temperature difference between A and B matters

S: Seebeck coefficient

n: Number of thermocouple junction pairs
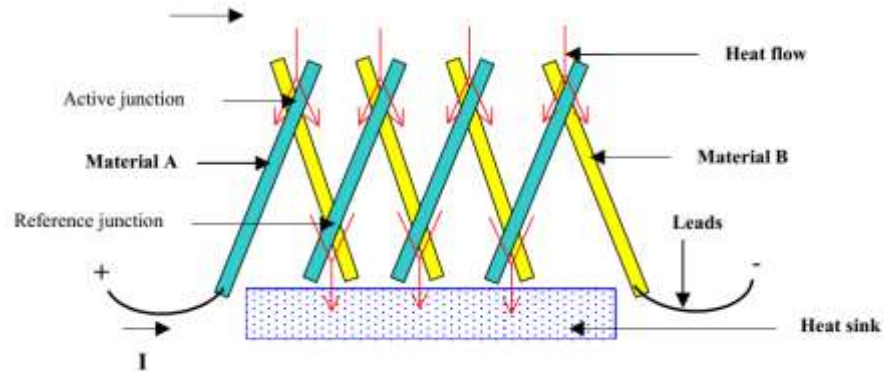
Figure 2.8 An illustration of a thermopile (Weckmann, 1997)

2.2.2.2 Pyroelectric Detectors

Pyroelectricity (from the Greek Pyr, fire, and electricity) is the ability of some specific crystals which produce a temporary voltage when they are heated or cooled. It can also be described as temperature variation dependence of the inherent polarization in specific anisotropic crystals. The materials that have such features are named pyroelectric materials, and the unit cells of this kind of materials have a dipole moment naturally. The spontaneous polarization (P_S) of pyroelectric crystals is determined as the dipole moment per unit volume of the material, and these crystals are permanently polarized within stable temperature.
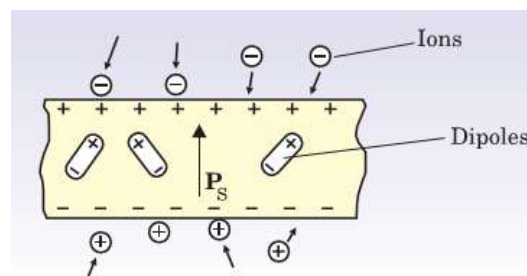
Figure 2.9 A pyroelectric crystal with an intrinsic dipole moment (Lang, 2005)

24

When the temperature of a pyroelectric crystal is kept constant, any occurring current flows through the circuit because no change can be seen in P_S. However, if the temperature of the crystal is increased, it causes the decreasing of the net dipole moment and the spontaneous polarization, P_S. As a result of this, the number of bound charges decreases, and to compensate for the change in bound charge, the redistribution of free charges creates a current flow that is named the pyroelectric current in the circuit. On the contrary to this event, if the temperature of the crystal is decreased instead of increasing, it causes the same result on crystal, but the current's sign is reversed. All of these steps define the pyroelectric effect. Besides, the important point here is that the pyroelectric effect can only be seen during the period in which the temperature changes. Otherwise, in an open circuit, the free charges of the crystal are expected to remain on the electrodes, so any voltage cannot be measured (Aggarwal, et. al., 2010; Pyroelectricity, n.d.).
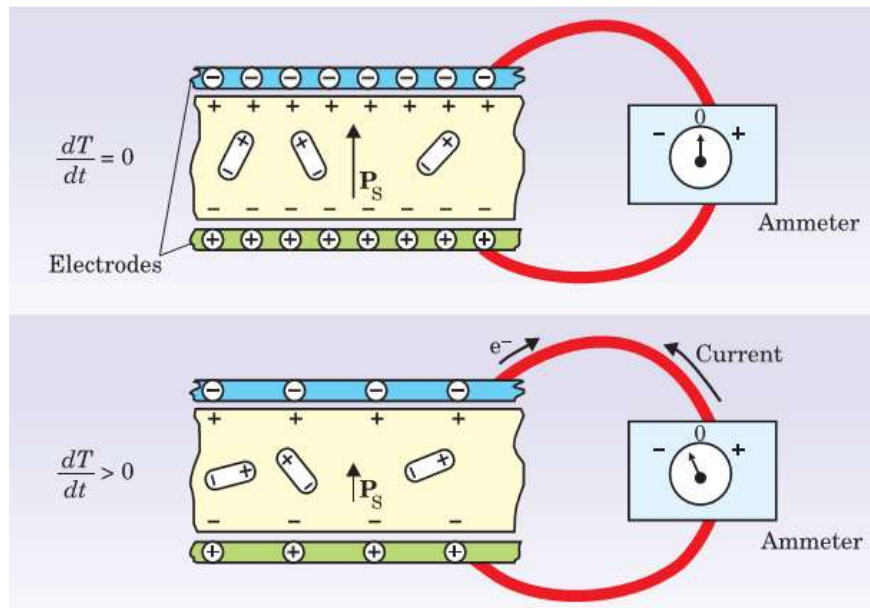
Figure 2.10 The pyroelectric effect (Lang, 2005)

When a temperature variation, ΔT, is uniformly applied to the crystal that shows a pyroelectric feature, the variation of the electric polarization, ΔP, is given by Equation 2.10.

$$\Delta P = \gamma \Delta T \qquad (2.10)$$

γ: the pyroelectric coefficient at constant stress

$$\gamma = \frac{\partial P_s}{\partial T} \quad \left[\frac{C}{m^2 K}\right] \tag{2.11}$$

The pyroelectric effect is a result of a migration of positive and negative charges (establishment of electric polarization) to opposite sides of the crystal's polar axis, because of the temperature variation. This can be represented by Equation 2.12. Also, the relation between produced charges and polarization is given by Equation 2.13.

$$\Delta Q = \gamma S \Delta T \tag{2.12}$$

ΔQ: charges generated on the crystal surface
S: surface of the crystal

$$Q = S\Delta P \quad \left[\frac{C}{m^2}\right] \tag{2.13}$$

All of these equations and the concept of the pyroelectric effect denote that if the temperature of the crystal is kept constant at its new value, the pyroelectric voltage gradually decreases owing to leakage current.

Moreover, the thermodynamic description of pyroelectricity can be explained as shown below.

$$P_k = P_k(T, \eta_{ij}, E_i) \, , \, \eta_{ij} = \eta_{ij}(T, \sigma_{lm}, E_i)$$

η_{ij}: Deformation
E_i: Electric field
σ_{lm}: Mechanical stresses

If $E_i = 0$, then changes of polarization and deformation can be written as Equation 2.14.

$$dP_k = \left(\frac{\partial P_k}{\partial T}\right)_{\eta_{ij}} dT + \left(\frac{\partial P_k}{\partial \eta_{ij}}\right)_T d\eta_{ij} \tag{2.14}$$

$$d\eta_{ij} = \left(\frac{\partial \eta_{ij}}{\partial T}\right)_{\sigma_{lm}} dT + \left(\frac{\partial \eta_{ij}}{\partial \sigma_{lm}}\right)_T d\sigma_{lm} \tag{2.15}$$

If the stresses are uniform, (σ_{lm} is constant), then, the total pyroelectric effect can be given by Equation 2.16 (Aggarwal, et. al., 2010); (Pyroelectricity, n.d.).

$$\left(\frac{\partial P_k}{\partial T}\right)_{\sigma_{lm}} = \left(\frac{\partial P_k}{\partial T}\right)_{\eta_{ij}} + \left(\frac{\partial P_k}{\partial \sigma_{lm}}\right)_{\eta_{ij}} \cdot \left(\frac{\partial \sigma_{lm}}{\partial \eta_{ij}}\right)_T \left(\frac{\partial \eta_{ij}}{\partial T}\right)_{\sigma_{lm}} \tag{2.16}$$

$\left(\frac{\partial P_k}{\partial T}\right)_{\sigma_{lm}} : \gamma_k^{\sigma}$ - *the total pyroelectric coefficient*

$\left(\frac{\partial P_k}{\partial T}\right)_{\eta_{ij}} : \gamma_k^{\eta}$ - *the primary pyroelectric coefficient*

$\left(\frac{\partial P_k}{\partial \sigma_{lm}}\right)_{\eta_{ij}} : d_{klm}^{\eta}$ - *the piezoelectric module*

$\left(\frac{\partial \sigma_{lm}}{\partial \eta_{ij}}\right)_T : C_{lmij}^{T}$ - *elastic compliance coefficients*

$\left(\frac{\partial \eta_{ij}}{\partial T}\right)_{\sigma_{lm}} : \alpha_{ij}^{\sigma}$ - *coefficients of thermal expansion*

Thus, Equation 2.16 can also be written as follows;

$$\gamma_k^{\sigma} = \gamma_k^{\eta} + d_{klm}^{\eta} C_{lmij}^{T} \alpha_{ij}^{\sigma} \tag{2.17}$$

The crystal of the pyroelectric thermal detector must be as thin as possible in order to sense the temperature changes rapidly. If the crystal is heated sufficiently, the electrical signal that has temperature information can be obtained faster, if the crystal has a smaller thermal time constant value. The thin pyroelectric crystals of the detectors are coated with appropriate 'black' absorber layers defined by an IR filter, to enhance the absorption rate of the incoming IR radiation. With the help of this IR filter, the IR radiation, which has a transmission rate μ_F, comes to the pyroelectric element. Then, the absorbed radiation flux, $\emptyset_0$, changes the temperature of the

crystal, ΔT. As can be seen, the pyroelectric effect causes thermal to electrical conversion that is because of the temperature change, ΔT which, varies the intensity of the charge ΔQ on the electrodes. At last, this electrical conversion allows to produce an electrical signal, Δu_S. Figure 2.14 (Detector basics, n.d.) shows this conversion steps schematically (Detector basics. n.d.).
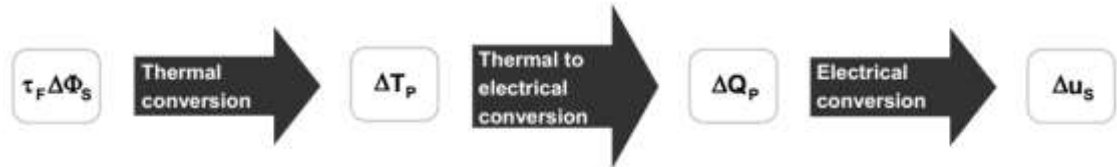
Figure 2.11 Conversion steps (Detector basics, n.d.)

In this chapter, currently used IR temperature measurement detector types were expressed simply. However, although general information about quantum detectors were given briefly for supplying theoretical information, the basic principles of the pyroelectric detectors and thermopile detectors were expressed in this chapter. Since, in this study, the detector that was used in designing the IR thermometer is a kind of thermopile thermal detector. Furthermore, the fundamental principles of pyroelectric detectors were clearly explained, owing to being a type of thermal detectors like thermopile detectors. The reason for using thermopile thermal detector in this study is that it can be obtained much more easily than pyroelectric detector.

CHAPTER THREE
DESIGN AND CONSTRUCTION

In this chapter, an IR body temperature measurement device that is illustrated in Figure 3.1 and Figure 3.2 is designed and constructed. In addition, this device can be used either connected or non-connected to a PC. This means the device can give temperature information via LCD or LCD and the computer's monitor as shown in Figure 3.4 (a) and (b). An important point of this situation is if the device is not connected to the PC, it must feed with a battery as shown in Figure 3.2.
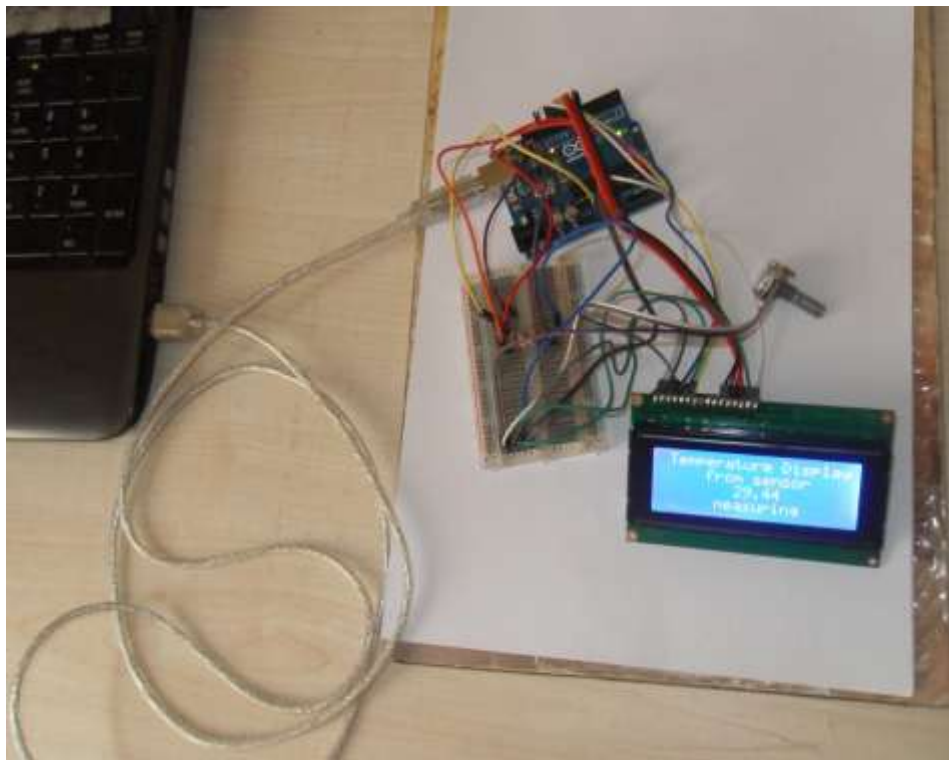
Figure 3.1 Constructed device connected to PC
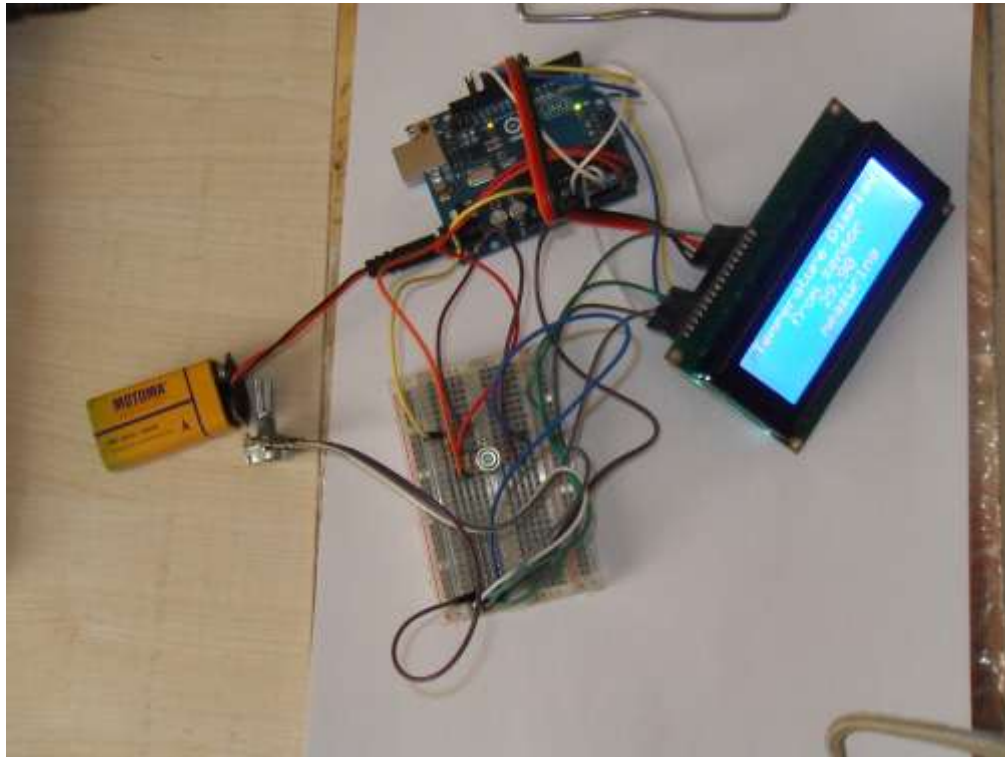
Figure 3.2 Constructed device is not connected to PC
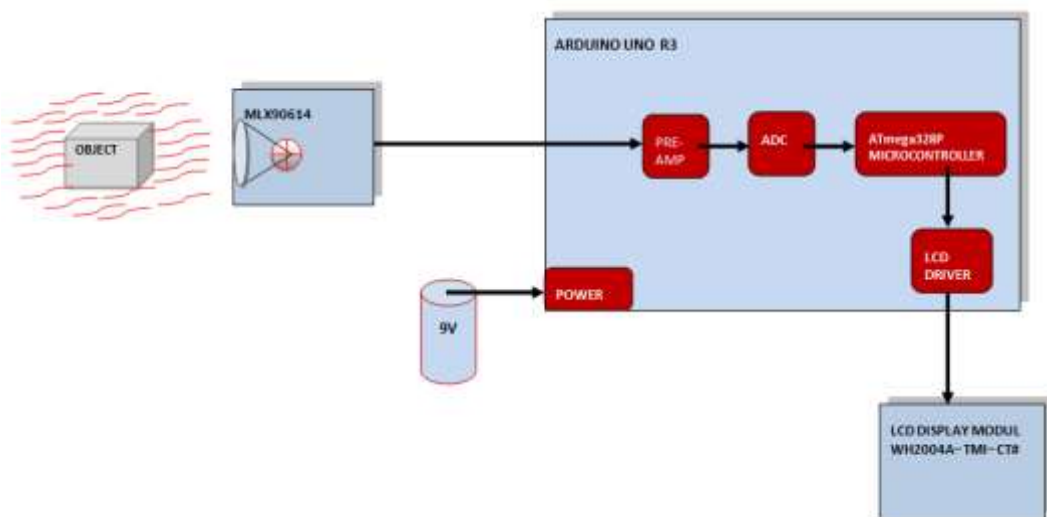
Figure 3.3 Block diagram of the constructed and designed device
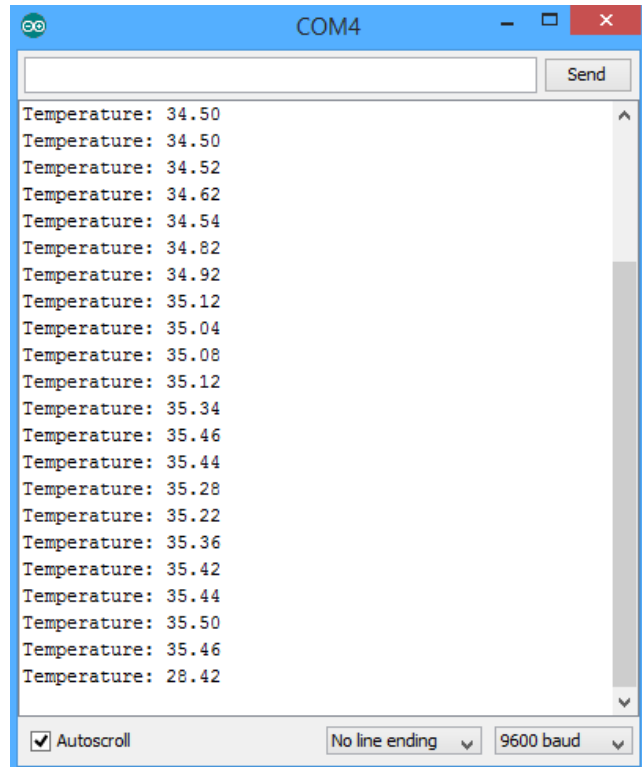
(a)
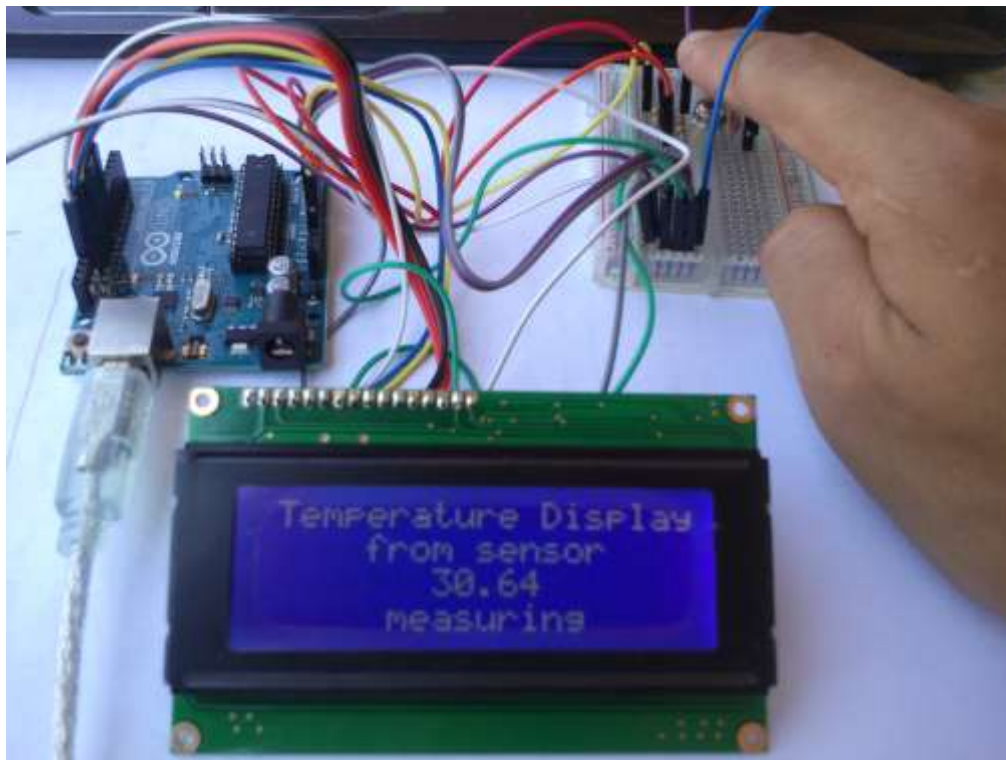
(b)

Figure 3.4 (a) Illustration of the sensor measurement on the PC monitor, and (b) illustration of the sensor measurement on the LCD

The main components of this constructed device have been shown and expressed below. These main components are the Microcontroller (Arduino; ATmega328P Microcontroller), IR radiation sensor (Melexis MLX9061), and LCD display module (WH 2004 A－TMI－CT#).

3.1 Microcontroller

The microcontroller that was used to construct the device is ATmega328P microcontroller which is embedded in the arduino. The ardunio which has an open source code is an electronic prototype that has a hardware and software structure, and it includes all required components on its board that as shown in Figure 3.5. It uses a distinctive programming language that is based on wiring. Because a "Bootloader" has been already loaded in its microcontroller, it does not need an external programmer. The bootloader is a general name of the software which was written on the EEPROM of the microcontroller of the arduino, and allows direct loading of commands that are written via serial communication into the microcontroller without using an external programming card.
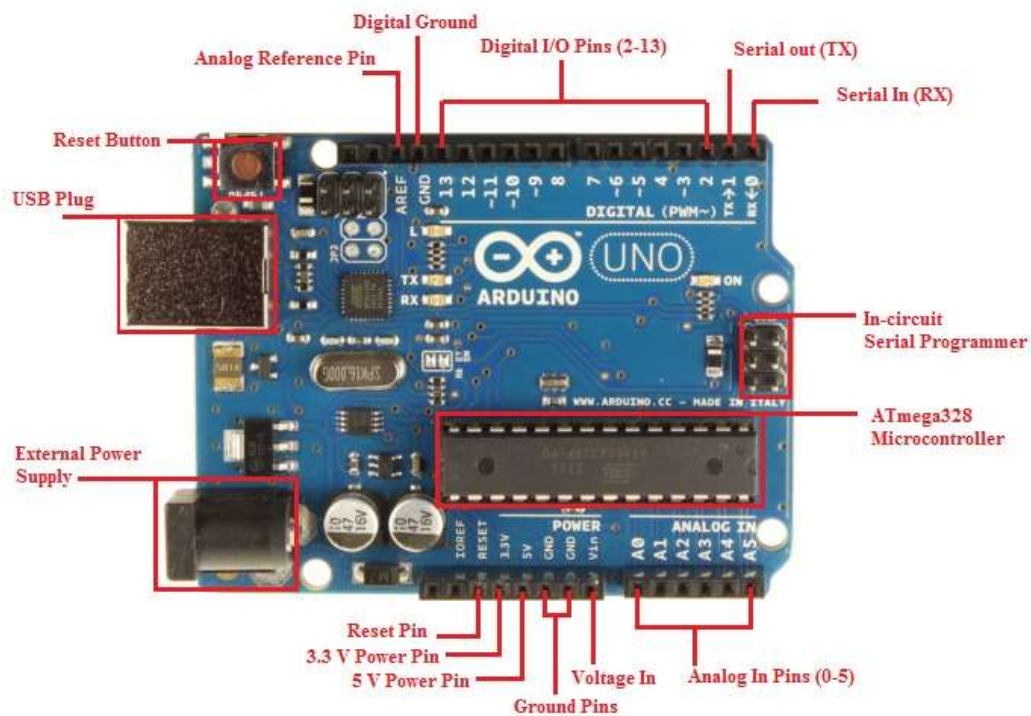
Figure 3.5 Arduino UNO R3
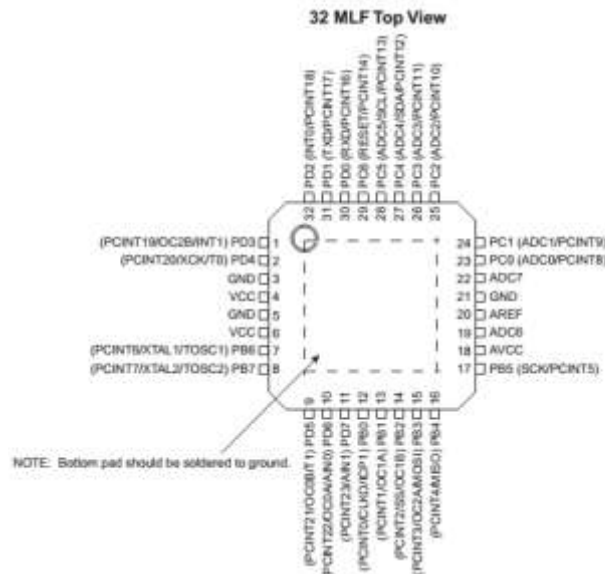
Figure 3.6 Pinout ATmega328P (Atmel Corporation (2009))

3.2 IR Radiation Sensor

In the constructed device, "Melexis MLX9061" IR sensor that is shown in Figure 3.7 (Melexis Microelectronic Systems, 2013) is used. The MLX90614 is an IR sensor to measure temperature of an object or environment as non-contact. In the MLX90614, a thermopile detector for perceiving the temperature difference of the object or the environment and a signal conditioning ASSP (Application Specific Standard Product) that is designed to process the output of the sensor are embedded in the same TO-39 can which is a kind of metal can package as shown in Figure 3.8 (Melexis Microelectronic Systems, 2013). A functional diagram of the sensor is also shown in Figure 3.9 (Melexis Microelectronic Systems, 2013).
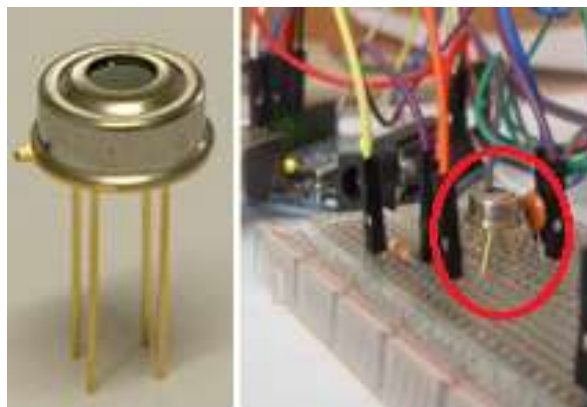
Figure 3.7 MLX90614 (Melexis Microelectronic Systems, 2013)

33

The reason for choosing this sensor for the construction was to achieve a high accuracy and resolution, due to its low noise amplifier, 17-bit ADC and a powerful DSP unit. Besides, the MLX90614 sensor does not need calibration since it comes factory calibrated in wide temperature ranges between -40 and 125°C for the environment temperature, and between -70 and 380°C for the object temperature with an output resolution of 0.14°C for both cases. That's why; it was not needed to calibrate the sensor during measurements.
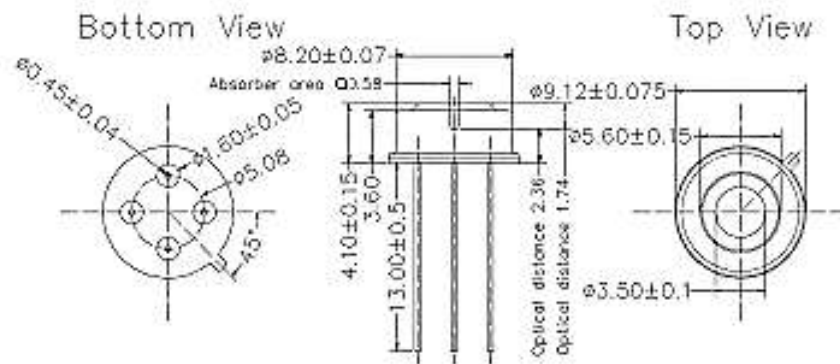
Figure 3.8 MLX90614 package (all dimensions are in mm) (Melexis Microelectronic Systems, 2013)

In the field of view (FOV) of the sensor, the temperature measurement that is read from the LCD of the device (or monitor of the computer) is an average value of the measured object. The standard accuracy of MLX90614 is about ±0.5°C for room temperatures, and for medical applications, the accuracy is about ±0.2°C in around the human body temperature. However, there is an important point that these accuracies are only available when the sensor is in thermal equilibrium and under isothermal conditions that means without any temperature difference across the sensor package. The temperature differences in the package can be a result of the hot electronics around the sensor, heaters/coolers neighboring of the sensor or a hot/cold object very near to the sensor. This effect can be minimized by choosing a smaller FOV or separating the sensor from the electronic parts of the system. FOV of this sensor is given 90° by datasheet of the sensor.
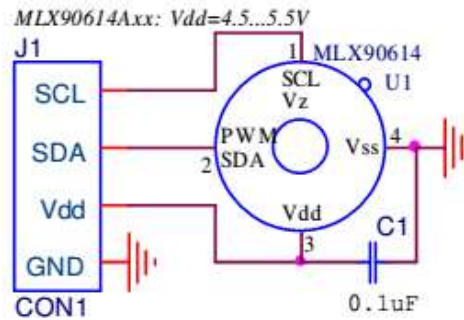
Figure 3.9 Functional diagram of the MLX90614 (Melexis Microelectronic Systems, 2013)

3.3 LCD Display Module

In the constructed device, WH 2004 A－TMI－CT# that is shown in Figure 3.10 is used as the LCD display module which is built in a LSI controller. The LSI controller has two 8-bit registers that are called an instruction register (IR) and a data register (DR).

The IR that can only be written from the MPU keeps the memory directive codes, such as cleaning display codes, and cursor shift, and directs information for the character generator (CGRAM) and display data RAM (DDRAM) that is used to store the display data represented in 8-bit character codes. On the other hand, the DR keeps data in the memory to be read or written from CGRAM or DDRAM temporarily. At first, the direction information is written into the IR, and after that, data is saved into the DR from CGRAM or DDRAM.
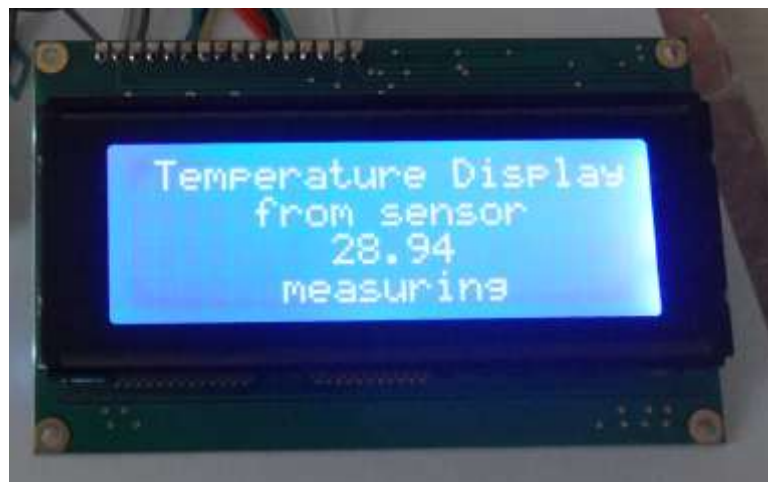
Figure 3.10 WH 2004 A－TMI－CT# LCD Module

35
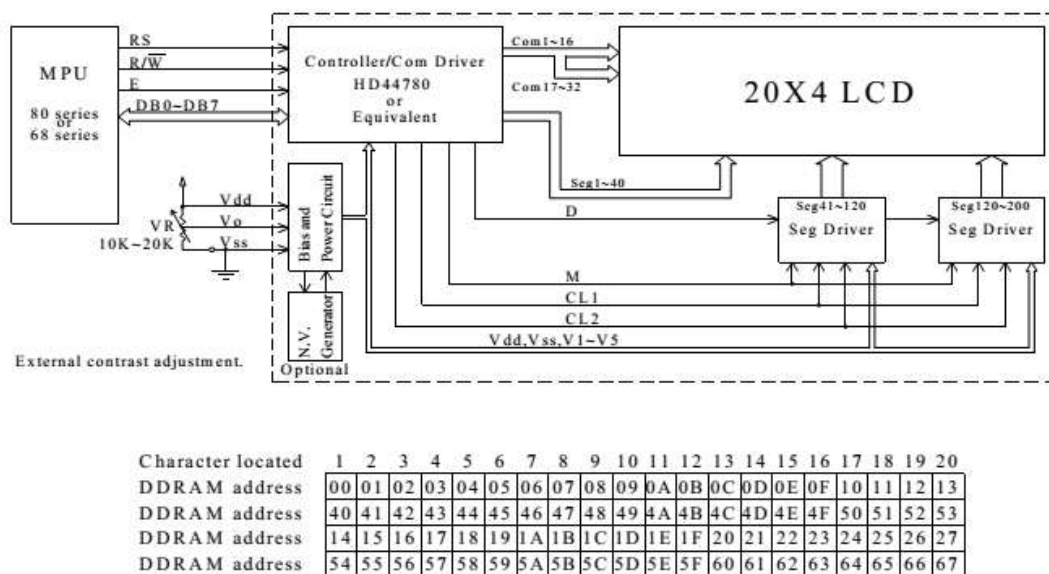
Figure 3.11 Block diagram of the WH 2004 A－TMI－CT# LCD module (Winstar Display Co., ltd., 2008)

Moreover, some features of IR measurement thermometers that can be found in the market are shown in Table 3.1.

Table 3.1 Some features of IR measurement thermometers in the market

IR Thermometer	Temperature range	Accuracy	Temperature work range	Spectral measurement range
Fluke 566	-40°C- 650 °C	<0°C(32°F): ± (1.0 °C (± 2.0 °F) >0°C(32°F): ±%1	0°C-50°C (32°F-122 °F)	8 μm - 14 μm
TFA 31.1114	-33°C - 250°C	±1,0°C	0°C-50°C	
Extech Instruments - IR200	23°C - 45 °C	+/- 0,3°C		
Optris - Mini Sight Pro	-32°C - 760°C	±1%	0°C-50°C	8 μm - 14 μm
Flash III	-55°C - 250°C	±2°C		
PCE-MF 1	-35°C - 250 °C	±2 °C	0°C-50°C	

CHAPTER FOUR
MEASUREMENTS AND COMPARISONS

In this study, a non-contact body temperature measurement device has been designed and constructed. After completing design and construction, two points of the body (axilla and palms) were selected and the body temperatures from these points of ten different people were measured. Furthermore, these measurements were repeated using a mercury thermometer, and a digital thermometer, and all values were compared.

Table 4.1 Temperature measurement values and standard deviations using three different measuring systems; measured temperature of palms (Tp), measured temperature of axilla (Ta), difference between mercury thermometer measurements and IR thermometer measurements for palms ($D1_{(p)}$), difference between digital thermometer measurements and IR thermometer measurements for palms ($D2_{(p)}$), difference between mercury thermometer measurements and IR thermometer measurements for axilla ($D1_{(a)}$), difference between digital thermometer measurements and IR thermometer measurements for axilla ($D2_{(a)}$)

Device	(Tp)	(Ta)	$D1_{(p)}$	$D2_{(p)}$	$D1_{(a)}$	$D2_{(a)}$
1-Mercury Thermometer	36.3°C	35.6°C	0.6	0	0.14	0.14
1-IR Thermometer	35.70°C	35.74°C				
1-Digital Thermometer	35.7°C	35.6°C				
2-Mercury Thermometer	35.9°C	36.8°C	0.06	0.16	0.08	0.08
2-IR Thermometer	35.84°C	36.88°C				
2-Digital Thermometer	36.0°C	36.8°C				
3-Mercury Thermometer	35.3°C	36.6°C	0.06	0.06	0.28	0.02
3-IR Thermometer	35.36°C	36.32°C				
3-Digital Thermometer	35.3°C	36.3°C				
4-Mercury Thermometer	36.3°C	36.0°C	0.16	0.34	0.2	0.3
4-IR Thermometer	36.14°C	36.20°C				
4-Digital Thermometer	35.8°C	35.9°C				

Table 4.1 (Continue)

5-Mercury Thermometer	36.0°C	36.2°C	0.12	0.12	0.04	0.04
5-IR Thermometer	36.12°C	36.24°C				
5-Digital Thermometer	36.0°C	36.2°C				
6-Mercury Thermometer	35.2°C	36.5°C	0.08	0.02	0.06	0.06
6-IR Thermometer	35.12°C	36.44°C				
6-Digital Thermometer	35.1°C	36.5°C				
7-Mercury Thermometer	36.0°C	36.3°C	0.08	0.08	0.08	0.08
7-IR Thermometer	36.08°C	36.38°C				
7-Digital Thermometer	36.0°C	36.3°C				
8-Mercury Thermometer	35.4°C	36.7°C	0.08	0.08	0.03	0.07
8-IR Thermometer	35.48°C	36.67°C				
8-Digital Thermometer	35.4°C	36.6°C				
9-Mercury Thermometer	35.2°C	36.2°C	0.02	0.12	0.12	0.07
9-IR Thermometer	35.18°C	36.32°C				
9-Digital Thermometer	35.3°C	36.3°C				
10-Mercury Thermometer	34.2°C	35.5°C	0.13	0.03	0.02	0.02
10-IR Thermometer	34.33°C	35.48°C				
10-Digital Thermometer	34.3°C	35.5°C				
Mean			0.139	0.0101	0.105	0.083
Standard Deviation			0.167	0.098	0.083	0.085

All measurements were performed under the following conditions: at 25°C room temperature and in a room with a size of 20m². Also, all measurements were taken at nearly 0.5 mm distance from the sensor. Measured values are listed as shown in Table 4.1. Using MATLABR2014a, their means and standard deviations are calculated as well. Table 4.1 shows that there are small differences between measurement values of the different measurement systems. However, it can be seen that the measurement from the axilla is more accurate than the measurement from the palms because of the environmental effects. In addition, measurement times of the systems are 1 second for IR thermometer, 60 seconds for a digital thermometer, and minimum 5 minutes for mercury thermometer. As a result, it is easy to see that some features of the IR thermometer make it more useful than the mercury thermometer, for instance, faster and easier measurement, quick repeatability, real time monitoring etc.

Table 4.2 Ages and genders of the people that provided the experimental measurements as volunteers

Age	Gender
25	Male
23	Male
22	Male
25	Male
24	Male
26	Female
23	Female
19	Female
22	Female
23	Female

Furthermore, a few objects' temperatures were measured from different distances to see the effect of distance on the measurement results. All measurements for all objects (ice cubes, a glass of tea, and a human hand) were repeated at five different distances (1cm, 2cm, 3cm, 5cm, and 10cm) from the IR sensor and all results are listed in Table 4.3. All measurement assemblies are shown in Figure 4.1, Figure 4.2 and Figure 4.3 for ice cubes, a glass of tea and a human hand respectively. In addition, in temperature measurement of the glass of tea, the temperature of tea was

not measured directly to prevent effect of the tea vapor. As it is shown in the measurement results the measurement distance is quite important for accuracy of measurement. If the distance is farther than 1cm it is seen as a meaningful difference between measurements. So, measurements should be taken from nearer than 1cm for accuracy of the measurement. However, due to the FOV of this sensor is 90°, if the measurement region is point, the chosen distance should be shorter than the 1cm.

Table 4.3 Measurements in different distances; T_{ice}: temperature of ice cubes, T_{tea}: temperature of a glass of tea, T_{hand}: temperature of a human hand

	T_{ice}	T_{tea}	T_{hand}
1cm	0.66 °C	64.48°C	35.18°C
2cm	3.74°C	60.86°C	33.78°C
3cm	10.56°C	50.62°C	32.90°C
5cm	15.20°C	45.58°C	32.16°C
10cm	21.32°C	33.26°C	29.82°C

Figure 4.1 Setup of IR temperature measurement of an ice cube

Figure 4.2 Setup of IR temperature measurement of a glass of tea
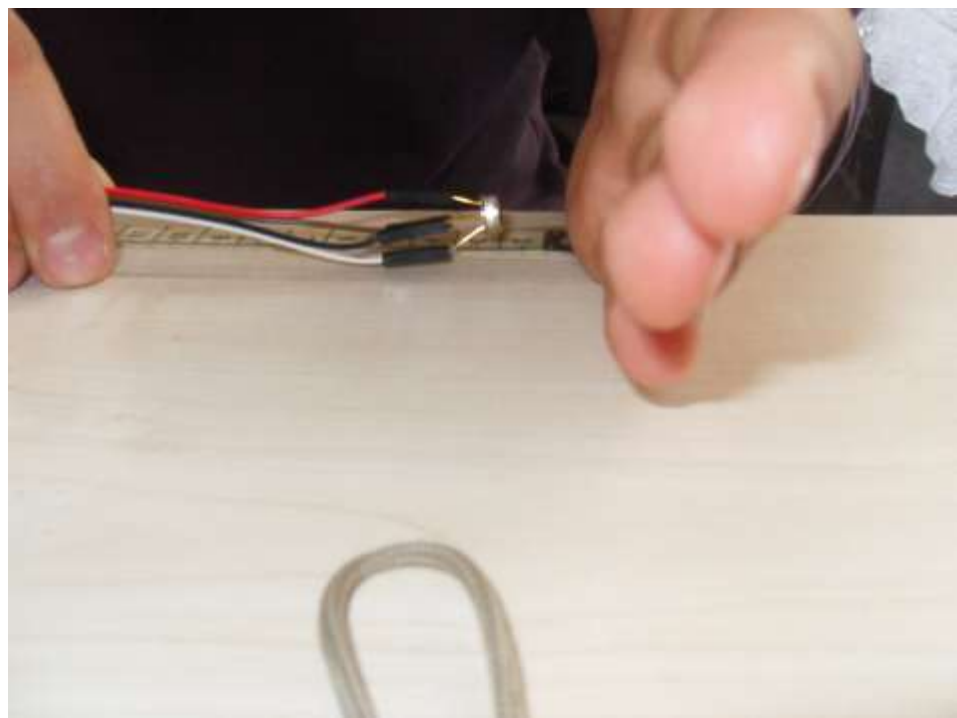

Figure 4.3 Setup of IR temperature measurement of a human hand

CHAPTER FIVE
CONCLUSIONS

IR radiation sensors are used widely in different fields such as electronics industry, machinery industry, and defense industry. In addition, nowadays, IR radiation sensors have started to be used in the medical industry day by day. In the medical industry, fast, easy and accurate temperature measurements are vital in terms of saving time. However, using the common body temperature measurement methods needs considerable time and effort.

In this study, designing and constructing an IR radiation thermometer has been purposed to measure body temperature using Melexis MLX90614 that is an IR radiation sensor based on thermopiles. Furthermore, in the design and construction steps, Arduino electronic prototype has been used with ATmega328P embedded microprocessor. Surely, it was needed to write a code to run this system, so it was written in the programming language that is based on wiring in Arduino.

As a result, the construction of the device has been completed and it has been used to measure body temperature as detailed in Chapter 3. When the device is compared to other measurement systems as it is seen in Chapter 4, it can be noticed that this device is more useful than the others owing to its speed, fast repeatability, easy usage, sensitivity, and real time monitoring. In addition, it measures the body temperature in a non-contact manner. This last feature provides a hygienic measurement that prevents infections between patients. Due to all of these advantages of the IR body temperature measurement device, it could be the most common method to measure body temperature in the near future.

REFERENCES

Aggarwal, M.D., Batra, A.K., Guggilla, P., Edwards, M.E., Penn, B.G., & Currie, J.R. (2010). *Pyroelectric materials for uncooled infrared detectors: processing properties, and applications.* Retrieved July 27, 2014, from http://ntrs.nasa.gov/archive/nasa/casi.ntrs.nasa.gov/20110008068.pdf

Atmel Corporation (2009). *ATmega48PA/88PA/168PA/328P datasheet*. Retrieved July 25, 2014 from http://www.atmel.com/Images/doc8161.pdf

Bronzino, J. D. (Ed.). (2006). *The biomedical engineering handbook (3rd ed.).* United States of America; CRC Press.

Detector basics. (n.d.). Retrieved July 25, 2014, from http://www.infratec.de/fileadmin/media/Sensorik/pdf/Appl_Notes/Application_Detector_Basics.pdf

Equipartition theorem, (n.d.). Retrieved October 24, 2014, from http://en.wikipedia.org/wiki/Equipartition_theorem#Translational_energy_and_ideal_gases.

Graf, A., Arndt, M., & Gerlach, G. (2007). *Seebeck's effect in micromachined thermopiles for infrared detection.* A review. Retrieved July 24, 2014, from http://www.kirj.ee/public/Engineering/2007/issue_4/eng-2007-4-7.pdf

Griffiths D. J. (2004). *Introduction to quantum mechanics (2nd ed.).* USA: Pearson Education Press

Harvey, D. (2008). *Modern analytical chemistry*. United States of America: The McGraw-Hill Companies

Hyseni, G., Caka, N., & Hyseni, K. (n.d.). *Analysis of MWIR infrared pyroelectric detectors parameters.* Retrieved July 27, 2014, from http://www.researchgate.net/publication/228375207_Analysis_of_MWIR_infrared_pyroelectric_detectors_parameters/file/32bfe50f941efb2a87.pdf

Infrared temperature measurement answers and solutions handbook, (n.d.). Retrieved July 22, 2014, from http://www.foxanddole.com/Infrared%20Temp%20Handbook.pdf

Introduction to thermopile detectors. (n.d.). Retrieved July 22, 2014, from http://www.lasercomponents.com/de/?embedded=1&file=fileadmin/userupload/home/Datasheets/drc/singleelements.pdf&no_cache=1

Johnson, C. (2012). *Mathematical physics of black body radiation.* Retrieved July 10, 2014, from http://www.csc.kth.se/~cgjoh/ambsblack.pdf

Jones, D. P. (2010). *Biomedical sensors.* New York: Momentum Press

Lang, S. B. (2005). *Pyroelectricity: From ancient curiosity to modern imaging tool.* Retrieved July 25, 2014, from *http://www.slac.stanford.edu/grp/arb/tn/arbvol5/AARD459.pdf*

Lawrence, J. D. (n.d.). *Thermopile sensors and applications to the detection of chemical and biological reactions and airborne pollutants.* Retrieved July 24, 2014 from http://www.cvaieee.org/html/past/081119_Sensors.pdf

Mallinckrodt, J., & Pomona, C. P. (2010). *Summary of black-body radiation theory and observations.* Retrieved May 16, 2014, from http://webcache.googleusercontent.com/search?q=cache:PeTKZmH3sAQJ:www.csupomona.edu/~ajm/classes/phy235/blackbody.pdf+&cd=1&hl=tr&ct=clnk&gl=tr

Melexis Microelectronic Systems (2013). *MLX90614 family single and dual zone infra red thermometer in TO-39 datasheet.* Retrieved August 12, 2014 from http://www.adafruit.com/datasheets/MLX90614.pdf

Optris GmbH. (n.d.). *Basic principles of non-contact temperature measurement.* Retrieved May 16, 2014, from http://www.optris.com.tr/tl_files/pdf/Downloads/Zubehoer/IR-Basics.pdf

Pyroelectric Infrared Detectors. (n.d.). Retrieved July 25, 2014, from http://www.dias-infrared.de/pdf/basics_eng.pdf

Pyroelectricity. (n.d.). Retrieved July 25, 2014, from http://gdp.if.pwr.wroc.pl/pliki/pyroelectric-effect.pdf

Pyroelectric detectors. (n.d.). Retrieved July 25, 2014, from http://www.infratec.de/fileadmin/downloads/pdf/behavior_of_detector_characteristics.pdf

Principles of non-contact temperature measurement, (n.d.). Retrieved July 22, 2014, from http://support.fluke.com/rayteksales/Download/Asset/IR_THEORY_55514_ENG_REVB_LR.PDF

Schilz, J., & Elmer, P. (n.d.). *Thermoelectric infrared sensors (thermopiles) for remote temperature measurements; pyrometry.* Retrieved July 22, 2014, from http://www.tuhh.de/mt/ftir/lib/RemoteTemperature/pyrometry.pdf

Sharkov, A. E. (2003). *Passive microwave remote sensing of the earth*. Germany; Praxis Publishing Ltd

Wang, P., & Li, Q. (2011). *Biomedical sensors and measurement*. Hangzhou; Zhejiang University Press

Weckmann, S. (1997). *Dynamic electro-thermal model of a sputtered thermopile thermal radiation detector for earth radiation budget applications*. Retrieved July 24, 2014 from http://ntrs.nasa.gov/archive/nasa/casi.ntrs.nasa.gov/20010117725.pdf

Widom, B. (2002). *Statistical mechanics: A concise introduction for chemists.* New York: Cambridge University Press

Winstar Display Co., ltd (2008). *WH2004A-CFH-JT# datasheet*. Retrieved August 12, 2014 from http://www.adafruit.com/datasheets/WH2004A-CFHJT%23.pdf

APPENDICES

Arduino Code of the Constructed Device

To run this designed and constructed temperature measurement device, the Arduino code given below is written and two libraries (i2cmaster.h and LiquidCrystal) that are presented by Arduino are used.

```
#include <LiquidCrystal.h>

#include <i2cmaster.h>

LiquidCrystal lcd(12, 14, 11, 7, 8, 9, 10);

void setup()

{

Serial.begin(9600);

Serial.println("Setup...");

 i2c_init(); //Initialise the i2c bus

PORTC = (1 << PORTC4) | (1 << PORTC5);//enable pullups

 lcd.begin(20, 4);

 lcd.setCursor(1,0);

 lcd.print("Temperature Display");

 lcd.setCursor(5,1);

 lcd.print("from sensor");

 lcd.setCursor(8,2);
```

```
  lcd.print("");

  lcd.setCursor(6,3);

  lcd.print("measuring");

}

void loop()

{

int dev = 0x5A<<1;

int data_low = 0;

int data_high = 0;

int pec = 0;

i2c_start_wait(dev+I2C_WRITE);

i2c_write(0x07);

i2c_rep_start(dev+I2C_READ);

data_low = i2c_readAck();

data_high = i2c_readAck();

pec = i2c_readNak();

i2c_stop();

double tempFactor = 0.02;

double tempData = 0x0000;
```

```
int frac;

tempData = (double)(((data_high & 0x007F) << 8) + data_low);

tempData = (tempData * tempFactor)-0.01;

float celcius = tempData - 273.15;

Serial.print("Temperature: ");

Serial.println(celcius);

  lcd.setCursor(1,0);

  lcd.print("Temperature Display");

  lcd.setCursor(5,1);

  lcd.print("from sensor");

  lcd.setCursor(8,2);

  lcd.print(celcius);

  lcd.setCursor(6,3);

  lcd.print("measuring");

delay(1000);

}
```

Maximum Ratings

Table 1. Absolute maximum ratings for MLX90614

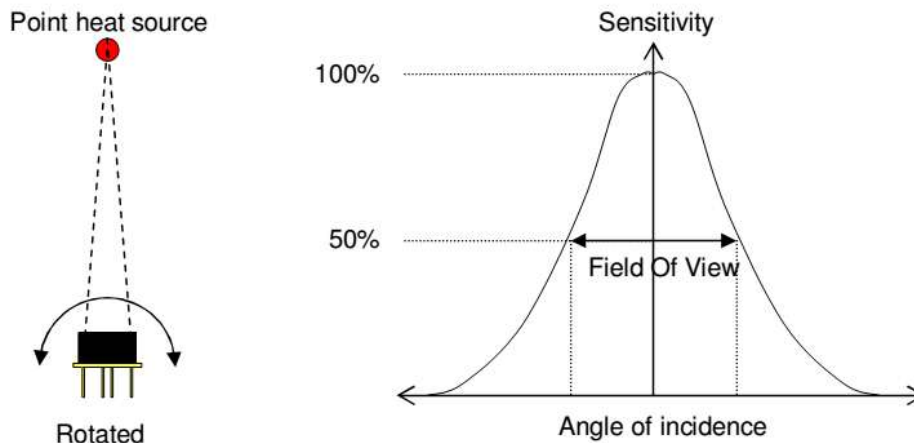| Parameter	MLX90614xAA
Supply Voltage, VDD (over voltage)	7V
Supply Voltage, VDD (operating)	5.5 V
Reverse Voltage	-40…+85C
Operating Temperature Range, TA	-40…+1 25C
Storage Temperature Range, TS	2kV
ESD Sensitivity (AEC Q1 00 002)	2 mA
DC current into SCL / Vz (Vz mode)	25 mA
DC sink current, SDA / PWM pin	25 mA
DC source current, SDA / PWM pin	25 mA
DC clamp current, SDA / PWM pin	25 mA
DC clamp current, SCL pin	25 mA

Field of View (FOV)

Figure 1 Field Of View measurement (Melexis Microelectronic Systems, 2013)

Table 2. FOV summary (Melexis Microelectronic Systems, 2013)

Parameter	MLX90614xAA
Peak Zone 1	±0°
Width Zone 1	90°
Peak Zone 2	Not applicable
Width Zone 2	

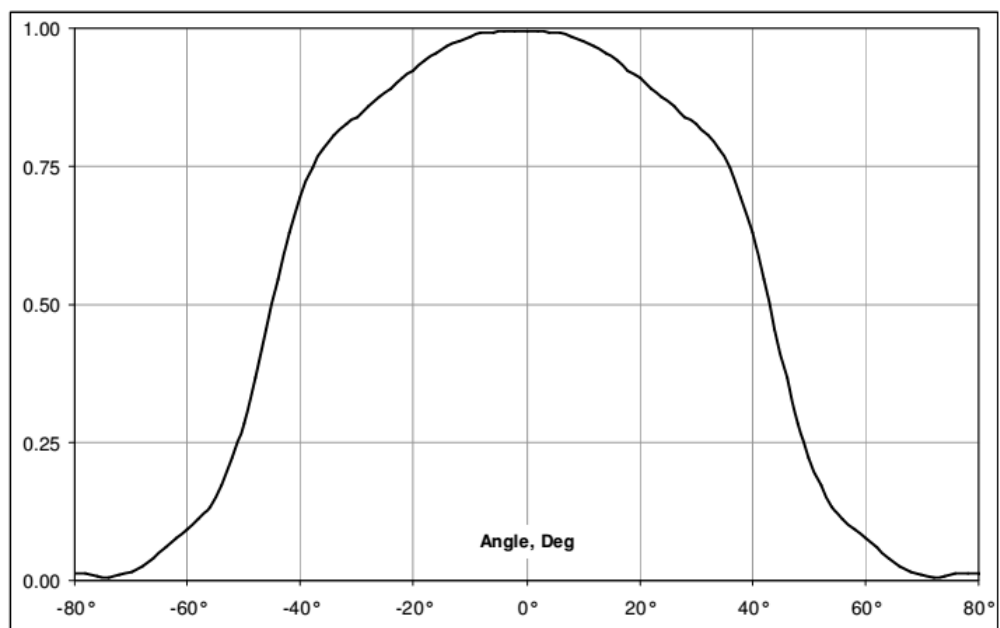Figure 2 Zones of the sensor (Melexis Microelectronic Systems, 2013)

Figure 3. Typical FOV of MLX90614xAA (Melexis Microelectronic Systems, 2013)